Nonsingular Implementation of the Mellor-Yamada Level 2.5 Scheme in the NCEP Meso model

by

Zaviša I. Janjić[1]

UCAR Scientific Visitor

December, 2001

National Centers for Environmental Prediction

Office Note #437

---

[1] *Corresponding Author's address: NOAA Science Center, WWB, Room 207, 5200 Auth Road, Camp Springs, MD, 20746; e-mail: zavisa.janjic@noaa.gov*

Summary

The Mellor and Yamada Level 2.5 scheme is analyzed in order to (i) identify the minimum conditions that enable satisfactory performance of the scheme in the full range of atmospheric forcing, and (ii) develop a robust, consistent, accurate and affordable computational procedure for application in synoptic and meso scale models. In order to achieve the first goal it is sufficient to impose an appropriate upper limit on the master length scale in addition to requiring that the turbulent kinetic energy (TKE) and the master length scale be positive. This upper limit is proportional to the square root of TKE and a function of buoyancy and shear of the driving flow. In the unstable range this function is defined from the requirement that the TKE production be nonsingular in the case of growing turbulence, and in the stable range the function is derived from the requirement that the ratio of the vertical velocity deviation variance and TKE cannot be smaller than that corresponding to the regime of vanishing turbulence. Thus, within the PBL the master length scale is estimated using the usual diagnostic formula, and above the PBL it is computed as a fraction of the vertical grid size. The values of the master length scale are then modified if necessary in order to satisfy the described constraint.

The TKE production/dissipation differential equation is solved iteratively over a time step. In each iteration, the differential equation obtained by linearizing around the solution from the previous iteration is solved. Two iterations appear to be sufficient for satisfactory accuracy, and the computational cost is minor.

The empirical constants have been revised. However, the techniques and methods of the study remain general, in the sense that they can be used with any other reasonably chosen set of constants.

The modifications have been tested in off-line runs and in an atmospheric model. Examples illustrating the performance of the scheme are presented.

1. Introduction

Over the last decade the Mellor-Yamada Level 2.5 model [e.g., Mellor and Yamada 1982 (hereafter referred to as MY82)] has become increasingly popular, presumably because of its conceptual appeal and straightforwardness, promising both accuracy in the treatment of the turbulent processes and efficient computational algorithm. Yet, the Level 2.5 model is known to have problems [e.g., MY82; Galperin et al. 1988; Helfand and Labraga 1988 (hereafter referred to as HL88); Janjić 1990 (hereafter referred to as J90); Gerrity et al. 1994 (hereafter referred to as GBT94)]. One should have in mind that the turbulence closure models are complex physical systems, so that the impact of the closure hypotheses on their internal consistency cannot always be fully anticipated. Therefore, the problems come as no surprise.

A comprehensive analysis of the Level 2.5 model was performed by HL88. However, they examined the realizability of the model in the space of stability and shear parameters that were dependent on both the turbulence variables and the large-scale driving flow. Although modestly stated, an important further step was made by GBT94 who examined the dependence of the turbulent kinetic energy (TKE) production on the gradient Richardson number. The gradient Richardson number was computed from the large-scale variables alone, which provided a clearer insight into the relationship between the turbulence and the driving flow.

An early response to the problems of the Level 2.5 model was to clip the buoyancy and shear parameters driving the turbulence [e.g., MY82, Eqs. (33a)-(33b), HL88, J90, Eqs. (3.6)]. Other possibilities have been examined as well, ranging from a modification of the model

(Galperin et al. 1988) to abandoning the Level 2.5 scheme in the case of growing convectively driven turbulence (HL88, GBT94).

The goals of the present study are (i) to define the minimum condition(s) that enable reasonable performance of the Level 2.5 scheme for the full range of atmospheric forcing, and (ii) to develop a robust, accurate, consistent and affordable computational procedure for its application in atmospheric models. To this end, the problems of the Level 2.5 model that are felt to be most important, and not yet sufficiently understood, will be reconsidered. Although the Richardson number covers the whole range of stability and shear, it has a singularity for the case of vanishing wind shear. In order to avoid a special treatment of this singularity, a two dimensional space will be used, with the stability and shear of the driving flow on the coordinate axes. In the context of the second of the stated goals, the question of the method used to solve the equation describing the contributions of the TKE production and dissipation will be addressed.

The results that will be presented have been obtained using a set of empirical constants which is different from that proposed in MY82. The new set of constants is derived in the Appendix. With these constants a better agreement with some important observed data is achieved. Nevertheless, the techniques and methods of the study remain general in the sense that they can be used with the MY82, or any other reasonably chosen set of constants, leading to analogous results.

2. The Mellor-Yamada Level 2.5 turbulence closure scheme

The Mellor-Yamada Level 2.5 turbulence closure model is governed by the equations (MY82):

$$\mathrm{d}(q^2/2)/\mathrm{d}t - (\partial/\partial z)[\ell\, q\, S_q\, (\partial/\partial z)(q^2/2)] = P_S + P_b - \varepsilon \tag{2.1}$$

$$P_S = -\langle wu\rangle\, (\partial U/\partial z) - \langle wu\rangle\, (\partial V/\partial z),\ P_b = \beta\, g\, \langle w\theta_v\rangle,\ \varepsilon = q^3/(B_1\, \ell) \tag{2.2}$$

$$-\langle wu\rangle = K_M\, \partial U/\partial z,\ -\langle wv\rangle = K_M\, \partial V/\partial z,$$

$$-\langle w\theta_v\rangle = K_H\, \partial \Theta_v/\partial z,\ -\langle ws\rangle = K_H\, \partial S/\partial z, \tag{2.3}$$

$$K_M = \ell\, q\, S_M,\ K_H = \ell\, q\, S_H, \tag{2.4}$$

$$S_M\, (6\, A_1\, A_2\, G_M) + S_H\, (1 - 3\, A_2\, B_2\, G_H - 12\, A_1\, A_2\, G_H) = A_2, \tag{2.5}$$

$$S_M\, (1 + 6\, A_1^2\, G_M - 9\, A_1\, A_2\, G_H) - S_H\, (12\, A_1^2\, G_H + 9\, A_1\, A_2\, G_H) = A_1\, (1 - 3\, C_1), \tag{2.6}$$

$$G_M = (\ell^2/q^2)[(\partial U/\partial z)^2 + (\partial V/\partial z)^2],\ G_H = -\,(\ell^2/q^2)\, \beta\, g\, \partial \Theta_v/\partial z. \tag{2.7}$$

Here, S_q=0.20, β=1/273, and the constants A_1, A_2, B_1, B_2 and C_1 are determined from experimental data and internal relations as discussed in more detail in MY82 and in the Appendix. The turbulent kinetic energy (TKE) is denoted by $q^2/2$, and ℓ is the master length scale yet to be determined. The variables describing the motions resolved by the atmospheric model are denoted by capital letters, and the lower case letters are used for the turbulent fluctuations. The subscript v is used to denote virtual potential temperature and S is a passive quantity. Note that the specific humidity is considered as a passive quantity within the framework of the model (2.1)-(2.7); the phase changes of atmospheric water affect the turbulence indirectly, through changes of the large-scale driving parameters. K_M and K_H are the vertical turbulent exchange coefficients for momentum and heat respectively and, as indicated by the subscript, P_S and P_b are the terms describing the production of the turbulent kinetic energy

due to shear and buoyancy. The dissipation is denoted by ε. Otherwise, the symbols have their usual meaning.

Several methods have been proposed for calculating the master length scale ℓ. However, this matter is not directly relevant for the considerations that will follow as long as a diagnostic formula is used for that purpose. A closer look at this problem will be postponed until the conditions that ℓ should satisfy are identified. It will suffice to say here that having defined the master length scale ℓ, G_M and G_H are calculated from (2.7), and S_M and S_H are then obtained solving the system (2.5)-(2.6). Now the exchange coefficients for momentum and heat (2.4) can be evaluated, and consequently the turbulent fluxes (2.3), and the forcing terms (2.2) on the right hand side of (2.1) can be obtained.

3. Parameter controlling production/dissipation of TKE

From (2.2), (2.3), (2.4) and (2.7), the contribution of the production/dissipation term may be rewritten in the form [c.f., e.g., J90, Eq. (3.7)]

$$P_s + P_b - \varepsilon = [S_M G_M + S_H G_H - 1/B_1] q^3/\ell. \tag{3.1}$$

Then, concentrating only to the contribution of the TKE production and dissipation, from (2.1) [c.f., J90, Eq. (3.10)-(3.11)]

$$\partial q/\partial t = (q^2/\ell) [S_M G_M + S_H G_H - 1/B_1]. \tag{3.2}$$

and,

$$(1/\ell) \partial q/\partial t = (q/\ell)^2 [S_M G_M + S_H G_H - 1/B_1]. \tag{3.3}$$

After rearrangement, (3.3) may be rewritten as

$$\ell\, \partial(1/q)/\partial t = - [S_M\, G_M + S_H\, G_H - 1/B_1]. \tag{3.4}$$

The procedure leading to (3.4) implies that q is positive. Apparently, an analogous assumption should be made for the master length scale ℓ. These two assumptions will be present throughout the considerations that follow.

Note that if local changes of the master length scale ℓ are neglected, as is usually done when using a separate (diagnostic) method for its computation, the master length scale may be placed under the differentiation sign on the left hand side of (3.4). Interpreting ℓ as a turbulence macro scale (e.g. MY82), in the case of well developed turbulence this can be justified by the (often implied) assumption that the characteristic time scale of the variation of ℓ is larger than that of q^2. A more pragmatic, and perhaps more general interpretation requiring no assumptions on the time scales, is that the diagnostic equation for ℓ and the prognostic equation for q^2 are simply solved in the split mode over the time step Δt.

In (3.4) the contribution of the TKE production terms is reflected by

$$S_M\, G_M + S_H\, G_H\,. \tag{3.5}$$

Denoting the determinant of the system (2.5)-(2.6) for S_M and S_H by Δ, and using the symbols $\Delta(S_M)$ and $\Delta(S_H)$ for the determinants obtained, respectively, by replacing the first and the second column of Δ by the right hand side column of (2.5)-(2.6),

$$S_M = -\Delta(S_M)/(-\Delta), \tag{3.6}$$

$$S_H = -\Delta(S_H)/(-\Delta)\,. \tag{3.7}$$

Thus, the contribution of the TKE production terms (3.5) can be rewritten as

$$S_M\, G_M + S_H\, G_H = -\,[\Delta(S_M)\, G_M + \Delta(S_H)\, G_H]/(-\Delta)\,. \tag{3.9}$$

Having in mind the definitions of G_M and G_H (2.7), and introducing new shear and stability parameters,

$$g_H = \partial\Theta_v/\partial z,\;\; g_M = (\partial U/\partial z)^2 + (\partial V/\partial z)^2, \tag{3.10}$$

after considerable, but straightforward algebra one obtains

$$(-\Delta) = 9\, A_1\, A_2\, (\beta\, g)\, g_H\, [2\, A_1\, (B_2 - 3\, A_2)\, g_M + A_2\, (12\, A_1 + 3\, B_2)(\beta\, g)\, g_H]\, (\ell/q)^4 +$$

$$+ 3\, [2\, A_1^2\, g_M + A_2\, (7\, A_1 + B_2)(\beta\, g)\, g_H]\, (\ell/q)^2 + 1, \tag{3.11}$$

$$\Delta(S_M) = -3\, A_1\, A_2\, (3\, A_2 + 3\, B_2\, C_1 + 12\, A_1\, C_1 - B_2)(\beta\, g)\, g_H\, (\ell/q)^2 + A_1\, (1 - 3\, C_1), \tag{3.12}$$

$$-\Delta(S_M)\, G_M = -\,[3\, A_1\, A_2\, (3\, A_2 + 3\, B_2\, C_1 + 12\, A_1\, C_1 - B_2)\, g_M\, (\beta\, g)\, g_H\, (\ell/q)^4 -$$

$$- A_1\, (1 - 3\, C_1)\, g_M\, (\ell/q)^2\,], \tag{3.13}$$

$$-\Delta(S_H) = A_2 + 9\, A_1\, A_2\, [A_2\, (\beta\, g)\, g_H + 2\, A_1\, C_1\, g_M]\, (\ell/q)^2, \tag{3.14}$$

$$-\Delta(S_H)\, G_H = -\{A_2\, (\beta\, g)\, g_H\, (\ell/q)^2 + 9\, A_1\, A_2\, [A_2\, (\beta\, g)^2\, g_H^2 +$$

$$+ 2\, A_1\, C_1\, g_M\, (\beta\, g)\, g_H]\, (\ell/q)^4\} \tag{3.15}$$

and finally, from (3.13) and (3.15),

$$-[\Delta(S_M)\, G_M + \Delta(S_H)\, G_H] =$$

$$[9\, A_1\, A_2^2\, (\beta\, g)^2\, g_H^2 + 3\, A_1\, A_2\, (3\, A_2 + 3\, B_2\, C_1 + 18\, A_1\, C_1 - B_2)\, g_M\, (\beta\, g)\, g_H]\, (\ell/q)^4 + \tag{3.16}$$

$$+ [A_1\, (1 - 3\, C_1)\, g_M - A_2\, (\beta\, g)\, g_H]\, (\ell/q)^2.$$

Thus, the numerator and the denominator of the expression on the right hand side of (3.9) are given by (3.16) and (3.11), respectively. Denoting the coefficients of $(\ell/q)^4$ and $(\ell/q)^2$ in (3.16) and (3.11) by

$$A = - [9\, A_1\, A_2^2\, (\beta\, g)^2\, g_H^2 + 3\, A_1\, A_2\, (3\, A_2 + 3\, B_2\, C_1 + 18\, A_1\, C_1 - B_2)\, g_M\, (\beta\, g)\, g_H], \qquad (3.17)$$

$$B = [A_1\, (1 - 3\, C_1)\, g_M - A_2\, (\beta\, g)\, g_H], \qquad (3.18)$$

$$C = 9\, [A_1\, A_2^2\, (12\, A_1 + 3\, B_2)(\beta\, g)^2\, g_H^2 + 2\, A_1^2\, A_2\, (B_2 - 3\, A_2)\, g_M\, (\beta\, g)\, g_H], \qquad (3.19)$$

$$D = 3\, [2\, A_1^2\, g_M + A_2\, (7\, A_1 + B_2)(\beta\, g)\, g_H], \qquad (3.20)$$

(3.4) can be rewritten as an ordinary differential equation

$$\ell\, \mathrm{d}(1/q)/\mathrm{d}t = - \{[A\, (\ell/q)^4 + B\, (\ell/q)^2]/[C\, (\ell/q)^4 + D\, (\ell/q)^2 + 1] - 1/B_1\}. \qquad (3.21)$$

Recalling that q and ℓ are positive, the evolution of TKE may have singularities depending on the ratio (ℓ/q) appearing as the only independent variable on the right hand side of (3.21). Therefore this ratio is the parameter that controls the TKE production in (2.1). The contribution of the dissipation term in (3.21) is reflected by the constant $1/B_1$, so that the dissipation poses no problem. Note that (ℓ/q) has the dimension of time. It is sometimes called "return to isotropy time" (e.g., Canuto et al. 1994)

The stability and shear parameters (3.10) depend entirely on the large-scale driving flow. Thus, for the reasons pointed out in the introductory section, the singularity problem will be further examined in the g_H x g_M plane.

4. The non-singularity constraint for the TKE production

The singularity problem of the Mellor-Yamada Level 2.5 model visibly manifests itself when trying to solve the algebraic equations (2.5)-(2.6). In the unstable case, the determinant of the system (3.6) may approach zero, so that the denominator (3.11) on the right hand side of (3.9) may vanish. Recalling the definitions of C (3.19), and B (3.20), this condition can be written in the form

$$(-\Delta) = C\,(\ell/q)^4 + B\,(\ell/q)^2 + 1 = 0. \tag{4.1}$$

Evaluation of the discriminant of (4.1) using the constants A_1, A_2, B_1, B_2 and C_1 derived in the Appendix shows that it is positive in the relevant part of the g_H x g_M plane, except at the coordinate origin g_H=g_M=0 where it vanishes. Therefore, (4.1) has two real roots for $(\ell/q)^2$, except at the coordinate origin where it has one.

It is also useful to find the equilibrium solution for $(\ell/q)^2$, i.e., the solution for which the TKE production is exactly balanced by the dissipation. Recall that the Mellor-Yamada Level 2 turbulence closure scheme is derived from the Level 2.5 model assuming that the production and the dissipation are always balanced (MY82). If an equilibrium solution exists, that will be a non-singular value of (ℓ/q). Then, as in GBT94, a root of (4.1) can be assumed to define the condition for non-singularity if there are no nonsingular solutions between that root and the equilibrium solution.

From (3.4), the requirement for the equilibrium has the form

$$S_M\,G_M + S_H\,G_H - 1/B_1 = 0. \tag{4.3}$$

Using again (3.11) and (3.16), the condition (4.3) may be rewritten as

$$E\,(\ell/q)^4 + F\,(\ell/q)^2 + 1 = 0, \tag{4.4}$$

where

$$E = [9\,A_1\,A_2^2\,B_1 + 9\,A_1\,A_2^2\,(12\,A_1 + 3\,B_2)](\beta\,g)^2\,g_H^2 +$$

$$+ [3\,A_1\,A_2\,B_1\,(3\,A_2 + 3\,B_2\,C_1 + 18\,A_1\,C_1 - B_2) + 18\,A_1^2\,A_2\,(B_2 - 3\,A_2)]\,g_M\,(\beta\,g)\,g_H \tag{4.5}$$

$$F = [3\,A_2\,(7\,A_1 + B_2) + A_2\,B_1](\beta\,g)\,g_H + [6\,A_1^2 - A_1\,B_1\,(1 - 3\,C_1)]\,g_M. \tag{4.6}$$

As before, evaluation of the discriminant of (4.4) using the constants A_1, A_2, B_1, B_2 and C_1 derived in the Appendix shows that it is positive in the relevant part of the g_H x g_M plane, except at the coordinate origin g_H=g_M=0 where it vanishes. Therefore, (4.4) has two real roots for $(\ell/q)^2$, except at the coordinate origin where it has one.

Analyzing the quadratic equations (4.4) and (4.1), one may notice that their respective leading coefficients E, defined by (4.5), and C, defined by (3.19), may vanish within the relevant range of the parameters g_M and g_H with the constants A_1, A_2, B_1, B_2 and C_1 derived in the Appendix. In order (i) to avoid special treatment of these singularities, and (ii) to facilitate the comparison with the results of GBT94, it is more convenient to use the equations equivalent to (4.1) and (4.4) for the reciprocal of $(\ell/q)^2$, i.e., for $(q/\ell)^2$. In this way, instead of (4.1) and (4.4) one obtains, respectively,

$$(q/\ell)^4 + D\,(q/\ell)^2 + C = 0, \tag{4.8}$$

and

$$(q/\ell)^4 + F\,(q/\ell)^2 + E = 0. \tag{4.9}$$

Here, the constants C, D, E and F are defined by (3.19), (3.20), (4.5) and (4.6) as before. Note that the discriminants of the equations (4.8) and (4.9) are the same as those of the equations (4.1)

and (4.4). Therefore, the results obtained analyzing the discriminants of the equations (4.1) and (4.4) are also applicable to the equations (4.8) and (4.9).

The solutions of the non-singularity condition equation (4.8), p_1 (upper panel) and p_2 (lower panel) are shown in Fig. 1 for the constants A_1, A_2, B_1, B_2 and C_1 derived in the Appendix, and a very wide range of g_H and g_M [$\pm 1^o$ K m^{-1} and (2 m s^{-1} m^{-1})^2, respectively]. The solutions p_1 and p_2 correspond to the roots with the plus and the minus sign in front of the square root, respectively.

The solutions of the TKE equilibrium equation (4.9) s_1 (upper panel) and s_2 (lower panel) are shown in Fig. 2 for the constants A_1, A_2, B_1, B_2 and C_1 derived in the Appendix, and the same range of g_H and g_M [$\pm 1^o$ K m^{-1} and (2 m s^{-1} m^{-1})^2, respectively]. The solutions s_1 and s_2 correspond to the roots with the plus and the minus sign in front of the square root, respectively.

As can be inferred analyzing the solutions of (4.8), as well as from Fig 2, s_1 is greater than s_2. In addition, contrary to what one would expect from the equilibrium solution, s_2 is negative for stable stratification. In contrast to that, s_1 is positive almost everywhere in the considered range of g_H and g_M. Thus, s_1 is identified as the actual equilibrium solution of the Mellor-Yamada Level 2.5 model. Also, as can be verified comparing the solutions, s_1 is always larger than p_1 within the considered range.

However, s_1 can also be negative, i.e., a physically meaningful equilibrium solution may not exist in a part of the g_H x g_M plane corresponding to very strong stability and/or very weak wind shear. Therefore, within the framework of the Level 2.5 model, the turbulence cannot be maintained in the range where s_1 is negative. Note that the vanishing equilibrium solution of (4.9) $s_1=(q/\ell)^2=0$ implies that the free term in (4.9) must also vanish, i.e., that

$$E = 0. \tag{4.10}$$

Having in mind the definition of E (4.5), and introducing the constants

$$a_{eH} = [9\, A_1\, A_2^2\, B_1 + 9\, A_1\, A_2^2\, (12\, A_1 + 3\, B_2)](\beta\, g) \tag{4.11}$$

$$a_{eM} = 3\, A_1\, A_2\, B_1\, (3\, A_2 + 3\, B_2\, C_1 + 18\, A_1\, C_1 - B_2) + 18\, A_1^2\, A_2\, (B_2 - 3\, A_2), \tag{4.12}$$

the condition (4.10) defines a straight line in the g_H x g_M plane

$$a_{eH}\, g_H + a_{eM}\, g_M = 0 \tag{4.13}$$

with the slope

$$R_{eq} = - a_{eH}/a_{eM}\,, \tag{4.14}$$

so that (4.13) can be rewritten as

$$g_M = R_{eq}\, g_H. \tag{4.15}$$

Thus, the turbulence cannot be maintained in the g_H x g_M plane below the line (4.15). Note that (4.15) also includes the coordinate origin point g_H=g_M=0. For the constants A_1, A_2, B_1, B_2 and C_1 derived in the Appendix,

$$R_{eq}=0.071139700558869442. \tag{4.16}$$

Contrary to the usual practice, the constant (4.16), as well as other constants defined later on, are given with a large number of significant digits in order to ensure reproducibility of the numerical results. As a matter of curiosity, having in mind the definitions of g_H and g_M (3.10), it follows from (4.16) that with the new constants the nonzero equilibrium solutions are possible for $Ri \leq 0.505$. In the case of the original MY82 constants, this limit is 0.193.

As can be seen analyzing the solutions of (4.8), as well as from Fig. 1, p_1 is nonnegative in the unstable and neutral range, and it is always greater than p_2. The root p_2 is negative almost

everywhere in the considered part of the g_H x g_M space. As can be readily verified, with p_1 greater than p_2, and s_1 greater than p_1 in the unstable and neutral ranges, there are no singular solutions between p_1 and s_1, which also points to p_1 as the root that defines the non-singularity. Thus, p_1 is left for imposing a physically meaningful non-singularity condition on $(q/\ell)^2$ in the unstable and neutral ranges.

The equilibrium solution s_1 being larger than p_1 indicates that the singularity related to the root p_1 is associated with growing turbulence (HL88, GBT94), i.e., with the situation where the equilibrium level s_1 has not been reached. For stable stratification, the implied assumptions that ℓ and q are positive appear to be sufficient for the non-singularity of the TKE production term. Thus, the non-singularity condition for the TKE production term can be written in the form

$$q/\ell > (p_1)^{1/2}, p_1 \geq 0 \text{ and } q, \ell > 0, p_1 < 0,$$

or returning to the reciprocal ℓ/q,

$$\ell/q < (1/p_1)^{1/2}, p_1 \geq 0 \text{ and } \ell, q > 0, p_1 < 0. \quad (4.17)$$

The values of the upper bound $1/p_1$ for $(\ell/q)^2$ for $p_1 \geq 0$ are displayed in Fig. 3 for the constants A_1, A_2, B_1, B_2 and C_1 derived in the Appendix, and the same wide range of g_H and g_M as before [$\pm 1^o$ K m^{-1} and (2 m s^{-1} m^{-1})^2, respectively].

5. The ratio $\langle w^2 \rangle / q^2$ in the stable range

As pointed out in Section 4, the non-singularity condition for the TKE production term has been related to the regime of growing turbulence in the unstable range. It may be interesting to

examine whether some useful information about the internal model relationships can be extracted in the case of vanishing turbulence in the stable range.

Introducing the symbol R_S for the ratio $<w^2>/q^2$, one may write [MY82, Eq. (37)],

$$R_S = <w^2>/q^2 = 1/3 - 2\, A_1\, S_M\, G_M + 4\, A_1\, S_H\, G_H. \tag{5.1}$$

Note that in the stable range both non-constant terms on the right hand side of (5.1) act in the direction of reducing the ratio R_S. Therefore, it may be interesting to find out what is the limit on the ratio (5.1) in the case of vanishing TKE along the line (4.15) where the equilibrium solution s_1 vanishes. This limit will be denoted by R_{SL}.

Substituting (3.6) and (3.7) into (5.1), and using the definitions (3.11), (3.13) and (3.15), one obtains

$$[27\, A_1\, A_2^2\, B_2\, (\beta\, g)^2\, g_H^2 + 54\, A_1^2\, A_2\, B_2\, C_1\, g_M\, (\beta\, g)\, g_H]\, (\ell/q)^4 +$$

$$+[18\, A_1^2\, C_1\, g_M + (9\, A_1\, A_2 + 3\, A_2\, B_2)(\beta\, g)\, g_H]\, (\ell/q)^2 + 1 = 3\, R_S\, (-\Delta)\,. \tag{5.2}$$

All terms on the left hand side of (5.2) are positive in the stable range ($g_H>0$), and, as can be readily verified, $(-\Delta)$ is positive if (4.17) is satisfied. Therefore, R_S must also be positive under the same conditions.

Using the definitions of C (3.19), and D (3.20), (3.11) can be rewritten as

$$(-\Delta) = C\, (\ell/q)^4 + D\, (\ell/q)^2 + 1,$$

so that (5.2) takes the form

$$\{[27\, A_1\, A_2^2\, B_2\, (\beta\, g)^2\, g_H^2 + 54\, A_1^2\, A_2\, B_2\, C_1\, g_M\, (\beta\, g)\, g_H] - 3\, R_S\, C\}\, (\ell/q)^4 +$$

$$\{[18\, A_1^2\, C_1\, g_M + (9\, A_1\, A_2 + 3\, A_2\, B_2)\, (\beta\, g)\, g_H] - 3\, R_S\, D\}\, (\ell/q)^2 + (1 - 3\, R_S) = 0. \tag{5.3}$$

Defining

$$G = \{[27\, A_1\, A_2^2\, B_2\, (\beta\, g)^2\, g_H^2 + 54\, A_1^2\, A_2\, B_2\, C_1\, g_M\, (\beta\, g)\, g_H] - 3\, R_S\, C\}, \quad (5.4)$$

$$H = \{[18\, A_1^2\, C_1\, g_M + (9\, A_1\, A_2 + 3\, A_2\, B_2)(\beta\, g)\, g_H] - 3\, R_S\, D\},$$

$$I = (1 - 3\, R_S),$$

(5.3) can be further rewritten as

$$G\, (\ell/q)^4 + H\, (\ell/q)^2 + I = 0, \quad (5.5)$$

or in terms of $(q/\ell)^2$,

$$I\, (q/\ell)^4 + H\, (q/\ell)^2 + G = 0. \quad (5.6)$$

Substituting the vanishing solution into (5.6), it is readily seen that the free term (5.4) of (5.6) must vanish, i.e., that

$$G = \{[27\, A_1\, A_2^2\, B_2\, (\beta\, g)^2\, g_H^2 + 54\, A_1^2\, A_2\, B_2\, C_1\, g_M\, (\beta\, g)\, g_H] - 3\, R_{sL}\, C\} = 0. \quad (5.7)$$

Introducing the constants,

$$a_{uH} = 27\, A_1\, A_2^2\, B_2\, (\beta\, g)^2,$$

$$a_{uM} = 54\, A_1^2\, A_2\, B_2\, C_1\, (\beta\, g),$$

(5.7) can be rewritten in a more compact form

$$a_{uH}\, g_H^2 + a_{uM}\, g_M\, g_H = 3\, R_{sL}\, C. \quad (5.8)$$

On the other hand, defining

$$a_{dH} = 9\, A_1\, A_2^2\, (12\, A_1 + 3\, B_2)(\beta\, g)^2,$$

$$a_{dM} = 18\, A_1^2\, A_2\, (B_2 - 3A_2)\, (\beta\, g),$$

(3.19) can be rewritten in the form

$$C = a_{dH}\, g_H^2 + a_{dM}\, g_M\, g_H,$$

so that, upon substitution in (5.8),

$$a_{uH}\, g_H + a_{uM}\, g_M = 3\, R_{sL}\, a_{dH}\, g_H + 3\, R_{sL}\, a_{dM}\, g_M$$

and

$$a_{uH} + a_{uM}\, g_M/g_H = 3\, R_{sL}\, a_{dH} + 3\, R_{sL}\, a_{dM}\, g_M/g_H. \tag{5.9}$$

The limit R_{sL} is reached along the line (4.15), so that substituting g_M/g_H from this equation into (5.9), and solving for R_{sL} one obtains

$$R_{sL} = (a_{uH} + a_{uM}\, R_{eq})/(3\, a_{dH} + 3\, a_{dM}\, R_{eq}). \tag{5.10}$$

Thus, (5.10) is the limit on the ratio $\langle w^2 \rangle / q^2$ corresponding to vanishing TKE along the line (4.15). For the constants A_1, A_2, B_1, B_2 and C_1 derived in the Appendix,

$$R_{sL}=0.1435678749111584933. \tag{5.11}$$

It will be assumed here that R_s cannot take on values below the limit R_{sL}.

With the constants A_1, A_2, B_1, B_2 and C_1 derived in the Appendix, and R_s close to R_{sL}, the discriminant of (5.5) is positive in the relevant part of the stable range of the g_H x g_M plane except at the coordinate origin $g_H=g_M=0$ where it vanishes. Therefore, (5.5) has two real roots

for $(\ell/q)^2$, except at the coordinate origin where it has one. Apparently, the same applies to the roots of (5.6).

The solutions of (5.6) t_1 (left panel) and t_2 (right panel) are shown in Fig. 4 for the constants A_1, A_2, B_1, B_2 and C_1 derived in the Appendix, $R_S=(1+10^{-12})R_{SL}$, and a very wide range of the stable part of the g_H x g_M plane [1° K m^{-1} and (2 m s^{-1} m^{-1})^2, respectively]. The solutions t_1 and t_2 correspond to the roots with the plus and the minus sign in front of the square root, respectively.

The solution t_2 is negative in the considered region, so that t_1 remains as the solution with possible physical significance. In addition, as long as R_S stays close to R_{SL}, s_1 is greater than t_1 except in the vicinity of the line (4.15) where the two solutions coincide for $R_S=R_{SL}$.

As can be seen from Fig. 4, the solution t_1 can also become negative for strong stability and/or weak wind shear. With the presently chosen constants, this happens along the line in the g_H x g_M space with the slope

$$0.07113970055869619755. \qquad (5.12)$$

Note that (5.12) is slightly smaller than (4.16), so that the range where t_1 is negative is a subset of the range where there is no positive equilibrium solution. As can be verified by direct inspection, the larger the value chosen for R_S, the larger is the value obtained for t_1. This explains the subtle difference between (4.16) and (5.12), the latter being obtained with R_S slightly larger than R_{SL}. However, as also can be directly verified, R_{SL} is the smallest single value of R_S for which t_1 remains nonnegative in the considered part of the stable range of the g_H x g_M plane in which the equilibrium solution s_1 is nonnegative. Thus, t_1 obtained for a suitably chosen value of R_S can again be used to impose a lower boundary on $(q/\ell)^2$ in the case of stable stratification, i.e., one may require that

$$q/\ell > (t_1)^{1/2}, p_1 < 0,$$

or returning to the reciprocal ℓ/q,

$$\ell/q < (1/t_1)^{1/2}, p_1 < 0. \tag{5.13}$$

As can be seen from Fig. 4, (5.13) is strongly affected by the shear, and much less so by the stability.

Note that HL88 imposed the lower bound of 0.12 on R_S following the MY82 argument that the Rotta hypothesis might fail for lower values. Here, a somewhat stricter criterion following from (5.11) has been obtained.

6. Summary of the restrictions on the master length scale following from the non-singularity condition and other considerations

Recalling the concluding remarks of Section 4 where p_1 was identified as the solution defining the non-singularity of the TKE production term in the unstable range, and the restriction on (ℓ/q) derived in Section 5 for stable stratification, a criterion of the form (4.17) can be extended also to the stable range, i.e., one may require

$$0 < \ell < a\, q \tag{6.1a}$$

where

$$a = (1/p_1)^{1/2}, \text{ for } p_1 \geq 0, \text{ and } a = (1/t_1)^{1/2}, \text{ for } p_1 < 0 \tag{6.1b}$$

The criterion (6.1) is not very strict for weak instability. In contrast to that, the restriction becomes severe in the stable range.

The non-singularity condition related to the root p_1 in the unstable range is associated with growing turbulence (HL88, GBT94), i.e., with the situation where the equilibrium level s_1 has not been reached. This condition implies that the master length scale should locally approach zero for vanishing turbulent kinetic energy.

In the stable range the criterion (6.1) formally resembles the widely used Deardorff's (1976) restriction on ℓ. However, unlike Deardorff's criterion which was based on considerations independent of the turbulence closure model, (5.13), and consequently (6.1) in the stable range, reflect an internal relationship inherent to the model. As a more substantive difference, one may note that the stability plays the key role in limiting ℓ in the Deardorff's criterion, while, as already pointed out, in the case of (5.13), and (6.1), the ratio of (ℓ/q) is strongly affected by the shear, and much less so by the stability.

If violated, the criterion (6.1) can be satisfied either by reducing the diagnostically computed ℓ, or by increasing TKE as was done e.g., by GBT94. Since the evolution of TKE is governed by a differential equation, changing TKE beyond the changes predicted by this equation would represent a deviation from the adopted turbulence closure model. Instead, it is postulated that the non-singularity condition should be applied in such a way that this equation always remains valid. Accordingly, the explanation of the problem proposed here is that in the case of growing turbulence the diagnostic method for calculating ℓ overestimates the master length scale in the unstable and neutral ranges for a given level of turbulent kinetic energy, leading to a violation of the criterion (6.1). The proposed interpretation suggests that the non-singularity problem in the unstable range should be controlled by restricting the diagnostically

computed master length scale ℓ using (6.1). By analogy, (6.1) is interpreted as the upper bound on ℓ in the stable range as well.

7. The time integration of the TKE production and dissipation term

In addition to the already considered problems, a method for solving (2.1) should be developed (c.f., e.g., Yamada 1986) in such a way as to guarantee a reasonable evolution of the solution. The dominating term in (2.1) is by far the TKE production/dissipation. Therefore, attention will be focused only to solving (3.21). As usual, in solving the equation for TKE, the master length scale is kept constant over the time step Δt. As already pointed out, this may be justified by the implied assumption that in the case of developed turbulence the time scale corresponding to the diagnostically computed integral quantity such as the master length scale is larger than that corresponding to a local variable such as q^2. A more pragmatic, and as will be pointed out later, more accurate interpretation under certain circumstances, is that the equations for ℓ and q^2 are simply solved in the split mode over the time step Δt. In accordance with these considerations, and for compactness, the master length scale will be written under the differentiation sign on the left hand side of (3.21), i.e., (3.21) will be rewritten in the form

$$\mathrm{d}(\ell/q)/\mathrm{d}t = -\{[A\,(\ell/q)^4 + B\,(\ell/q)^2]/[C\,(\ell/q)^4 + D\,(\ell/q)^2 + 1] - 1/B_1\}. \qquad (7.1)$$

Recall that the constants A, B, C and D are defined by (3.17)-(3.20).

The method proposed here is to linearize the right hand side of (7.1) with respect to ℓ/q, and then to iterate until the required accuracy is achieved. If the right hand side of (7.1) is denoted by R,

$$dR/d(\ell/q) = R' = -2\,[(A\,D - B\,C)\,(\ell/q)^5 + 2\,A\,(\ell/q)^3 + B\,(\ell/q)]/[C\,(\ell/q)^4 + D\,(\ell/q)^2 + 1]^2. \quad (7.2)$$

The iterative procedure can then be described using the linearized version of (7.1) by

$$d(\ell/q)_{i+1}/dt = R[(\ell/q)_i] + R'[(\ell/q)_i]\,[(\ell/q)_{i+1} - (\ell/q)_i], \quad (7.3)$$

where $(\ell/q)_i$ is the value of ℓ/q around which the linearization is performed. It seems natural to start the iterations linearizing (7.1) around ℓ/q corresponding to the equilibrium solution s_1 of the equation (4.8). For this value of ℓ/q, R=0, so that the solution of (7.1) should not go across the equilibrium, no matter from which side it tends to it. As can be easily verified, the solution of (7.3) has the form

$$(\ell/q)_{i+1} = (\ell/q)_i - R[(\ell/q)_i]/R'[(\ell/q)_i] +$$

$$\{R[(\ell/q)_i]/R'[(\ell/q)_i] + [(\ell/q)_0 - (\ell/q)_i]\}\,\exp\{\Delta t\,R'[(\ell/q)_i]\}, \quad (7.4)$$

where $(\ell/q)_0$ is the initial value of ℓ/q at the beginning of the time step Δt. Thus, in every subsequent iteration, the right hand side is linearized around the solution (7.4) obtained in the previous iteration, and the resulting linear differential equation is integrated starting always from the same initial value $(\ell/q)_0$.

It is not obvious that the procedure (7.2)-(7.4) converges, and if it does, how fast the convergence is. In order to answer these questions, a numerical test has been set up. For the choice of constants derived in the Appendix, (7.4) is solved starting from

$$(\ell/q)_0 = (1/p_1)^{1/2}/(1+10^{-12})^{1/2},\ p_1 \geq 0,$$

$$(\ell/q)_0 = (1/t_1)^{1/2} \text{ with } R_S=(1+10^{-12})\,R_{SL},\ p_1 < 0. \quad (7.5)$$

at the beginning of the time step Δt, i.e., at the limits specified by the criterion (7.1). The parameters R_S and R_{SL}, and the solution t_1, were discussed in detail in Section 5. For

computational reasons, if $|g_H|<\varepsilon_H=10^{-8}$, g_H is set to ε_H. The sign chosen for this artificial limit does not seem to matter. Note that its numerical value corresponds to the lapse rate of 1º C per one million kilometers. Similarly, g_M is not allowed to drop below $\varepsilon_M=R_{eq}\varepsilon_H$, where R_{eq} is defined by (4.14).

The number of iterations needed in order to obtain the solution of (7.4) using (7.5) is typically quite small. More iterations are needed if higher accuracy is to be achieved, particularly in the vicinity of the line (4.15) where the equilibrium solution s_1 vanishes. However, no convergence problems have been encountered in severe tests even if the difference between $(\ell/q)_{i+1}$ and $(\ell/q)_i$ is required to be at the eighth significant digit as the criterion for terminating the iterative procedure. In the range of the g_H x g_M plane where there is no equilibrium solution, the iterations are not made. For applications in atmospheric models, two iterations appear to be more than enough in order to obtain solutions with sufficient accuracy.

So far, the accuracy and efficiency of the procedure (7.4) have been commented on, but not the solutions obtained. In the unstable range, as a rule, when the convergence is reached within a single iteration, the solution corresponds to the equilibrium solution for the given master length scale ℓ and external forcing, measured, e.g., in terms of g_H and g_M. This does not necessarily mean that a steady equilibrium state is reached. In accordance with the considerations of Section 4, in the case of growing turbulence, it is natural to expect that the master length scale (computed diagnostically) will grow as well. Thus, even if the equilibrium solution is reached within the current time step, due to increase of ℓ, the equilibrium may again be violated in the next time step, so that the turbulence can grow by consecutive, split mode, increases of TKE and ℓ. Note that this scenario contradicts the assumption on different time scales for ℓ and q in the areas of fast growing turbulence.

8. The implementation

The described techniques have been implemented in a single column model, and in the NCEP Meso model (Chen et al. 1997; Janjić 1979, 1984, 1990, 1994; Mesinger et al. 1988; Zhao and Carr 1997). As in J90, the large-scale variables are defined in the middle of the model layers, whereas the turbulence parameters are carried at the interfaces of the layers. However, compared to J90, the order of the computations has been changed. The master length scale is determined first, and then the contribution due to the production and dissipation terms is added to TKE. The diffusion coefficients are computed using the updated TKE, but without recomputation of the master length scale. The vertical diffusion of TKE is postponed until after the computation of the turbulent exchange coefficients. Due to the linearization of the production/dissipation equation (7.3) and the iterative procedure used, practically the same parameters determine the TKE production/dissipation and the vertical diffusion of the large scale variables. More precisely, q_i determines the evolution of TKE, while q_{i+1} enters the exchange coefficients. However, due to fast convergence of the procedure (7.3)-(7.4), the difference between q_i and q_{i+1} should be small.

For the preliminary value of the master length scale within the PBL, the diagnostic formula of the form (e.g., MY82)

$$\ell = \ell_0 \, kz/(kz + \ell_0) \, , \quad \ell_0 = \alpha \int_0^{H_{PBL}} (|z| \, q \, dz) \Big/ \int_0^{H_{PBL}} (q \, dz) \, , \quad \alpha = \text{const} \, , \tag{8.1a}$$

is used. In (8.1a), H_{PBL} is the PBL height, k is the von Karman constant, and α is an empirical constant set to 0.25 in the tests. According to (8.1a), ℓ tends to kz for small z, and to the

asymptotic integral value ℓ_0 for large z. The PBL height is defined as the lowest model level above the surface at which the equilibrium turbulent energy s_1 becomes negative, or alternatively, as the height of the lowest model level at which TKE approaches its prescribed lower bound. Following Mason (1989), above the PBL the master length scale is computed as a fraction of the model grid distance Δz, i.e.,

$$\ell = 0.23\ \Delta z \tag{8.1b}$$

The values obtained either from (8.1a), or (8.1b) are then modified if necessary in order to satisfy the criterion (7.1).

A surface layer formulated following the similarity theory (Monin and Obukhov 1954) is used to provide the lower boundary conditions for the Level 2.5 model (Janjić 1996). The Beljaars (1994) correction is applied in order to avoid singularities in the case of free convection and vanishing wind speed (and consequently $u*$). With this correction, a fraction of the surface buoyancy flux is converted into kinetic energy of unorganized flow near the surface, so that the friction velocity $u*$ is never identically equal to zero. Anticipating the use of the radiative skin temperature instead of near surface air temperature as the lower boundary condition, a viscous sublayer parameterization recently proposed by Zilitinkevitch (1995) is used. With this parameterization, the temperature and humidity roughness height z_{0T} is defined in terms of the roughness height for momentum z_{0M} as

$$z_{0T} = z_{0M} \exp\left(- k\, C\, Re^{1/2}\right), \tag{8.2}$$

where C is an empirical constant $Re=z_{0M}u*/v$ is the *R*eynolds number, and v is the molecular viscosity for momentum. Over the ocean, the viscous sublayer is parameterized following Janjić (1994). The Paulson (1970) integral similarity functions are used over land, and the functions derived from the Mellor-Yamada Level 2 model by Lobocki (1993) are applied over water.

9. The tests

Emphasis is placed on the convective boundary layers since it is sometimes argued that the Mellor-Yamada Level 2.5 scheme has difficulties with unstable stratification. Generally, with the techniques proposed here, the large amplitude high frequency oscillations pointed out by HL88 and GBT94 do not characterize the simulated evolution of the turbulent variables. This point will be illustrated later on by an example from a real data run using the Meso model. In the mean time, results obtained in the idealized, single column tests will be examined.

(a) Single column tests

In the single column tests, the vertical resolution below 3264 m is chosen in such a way as to mimic the vertical resolution of the 38 layer Meso model for the points with no orography. Above the 3264 m interface, the depths of the layers used in the off-line tests do not change with height. The initial profiles of temperature, humidity and wind are prescribed as piece-wise linear functions of height. The temperature and humidity are constant (220º K and 0 kg/kg) from the top of the atmosphere to the first model level below 15000 m respectively, and then increase linearly as the height decreases, reaching the values of 290º K and 0.02 kg/kg at the ground surface. Note that such an atmosphere is rather stable. Similarly, if the wind speed is not specified to be zero, the velocity components are constant from the top to the first model level below 2000 m, and then decrease linearly with decreasing height, reaching zero at the surface.

In the tests over land points, the PBL is driven primarily by a cosine shaped diurnal cycle in the mean daily surface temperature. In fact, in order to simulate the extended duration of the solar heating on a summer day, the cosine curve is shifted upwards by 2.5º K, thereby increasing the mean surface temperature by the same amount. The amplitude of the cosine wave was 12.5º K, so that the full swing of the diurnal cycle was 25º K. The integrations started with the minimum in the cosine forcing, i.e., at the local "midnight". The surface latent heat flux was computed as 15% of the potential surface latent heat flux. The time step used was 400 s.

Since the model resolution is variable in the lower troposphere, and the PBL height changes during the day, the vertical distributions that will be shown are mapped at each time step from the model grid to a regular 20 point grid using cubic splines. The mapped data are then used to obtain the time averaged profiles.

In the free convection case, the initial large-scale wind is set to zero. Since there is no forcing other than the vertical turbulent transports, the large-scale wind field remains zero during the integration. The time averaged vertical distribution of the turbulent exchange coefficient for heat K_H normalized by the product of $w*$ and H_{PBL} is shown in Fig. 5 as a function of the normalized height z/H_{PBL}. As usual, the scale $w*$ is defined by

$$w* = [\beta\, g\, \langle w\theta_V \rangle_s H_{PBL}]^{1/3}$$

where $\langle w\theta_V \rangle$ is the surface buoyancy flux. For the data shown in the figure, the time averaging was performed over the period with the PBL height and the surface buoyancy flux exceeding 500 m, and 100 W m^{-2}, respectively. The PBL height reached the maximum of 1965 m in this test. Strictly speaking, $u*$ must have vanished because of the vanishing wind speed, so that $u*/w*=0$. However due to the Beljaars (1994) correction applied to the surface layer, the modified friction velocity $u*_B$ is greater than zero, and the average value of the modified ratio for the period

considered was $u*_B/w* = 0.139$. Note that the average profile shown in Fig. 5 qualitatively agrees with the profiles discussed in a different context e.g. by Holtslag and Moeng (1991). As in their study, the maximum value of about 0.1 is reached at about 0.4 z/H_{PBL}.

However, considering that the part of the atmosphere affected by the PBL has considerable thermal and dynamical inertia, the question arises as to whether the mean profile shown in Fig. 5 is stationary, and therefore equally representative for all stages of the diurnal history of a convective PBL. In order to find out what is the response of the model, the normalized profiles of K_H are plotted in Fig. 6 for more mature stages of the PBL development. In the figure, the average profile obtained for the PBL height and the surface buoyancy flux exceeding 1000 m and 100 Wm^{-2}, respectively, is denoted by squares, and the profile obtained for the maximum height of the PBL and the surface buoyancy flux greater than 100 W m^{-2} is denoted by triangles. The corresponding average ratios $u*_B/w*$ for these two cases were 0.136 and 0.133, respectively. For comparison, the profile of Fig. 5 denoted by circles is also included in the figure. Note that the scale of Fig. 6 has been changed compared to that of Fig. 5 in order to show more clearly the features of the profiles. As can be seen from the figure, the maximum increases, and shifts upwards as the PBL reaches maturity. Therefore, the model predicts nonstationary vertical profiles of K_H. It may also be noted in Fig. 6, that the exchange coefficients are taking on negative values. This is entirely an artifact of the spline interpolation. The values of K_H prior to the interpolation are always positive.

The average vertical buoyancy fluxes normalized by their surface values are shown in Fig. 7 as functions of normalized height z/H_{PBL} for the three regimes of the PBL considered. As can be seen from the figure, the profiles are reasonably close to a straight line up to about 0.9 z/H_{PBL}. At about this height the normalized fluxes become negative, but their absolute values are rather small, even though they are amplified by the spline interpolation. This is perhaps

something that should have been expected. The PBL height over a grid box of an NWP model is inhomogenous, so that the area mean of the vertical buoyancy flux profile should have the negative peak smeared.

In the case of convective boundary layer with shear, the initial large-scale wind was set to 10 m s^{-1} from the top to the first model level below 2000 m, and then the initial wind decreased linearly with decreasing height, reaching zero at the surface. The averaged vertical distribution of the turbulent exchange coefficient for heat K_H normalized by the product of $w*$ and H_{PBL} is shown in Fig. 8 as a function of the normalized height z/H_{PBL} for the PBL height and surface buoyancy flux exceeding 500 m and 100 W m^{-2} (circles), the PBL height and surface buoyancy flux exceeding 1000 m and 100 W m^{-2} (squares), and the PBL height greater than or equal to 1965 m and the surface buoyancy flux greater than 100 W m^{-2} (triangles). In the test H_{PBL} reached the maximum value of 2256 m. The values of the ratio $u*_B/w*$ for the three cases considered were respectively 0.154, 0.154 and 0.158. Although, the convection is now modified by shear, the profiles shown in Fig. 8 qualitatively agree with those corresponding to the free convection case shown in Fig. 6. As can be seen from Fig. 8, the maximum again increases and shifts upwards as the PBL reaches maturity, i.e., the model once more predicts non-stationary vertical profiles of K_H. The negative values of K_H are again produced by the spline interpolation.

The average vertical buoyancy flux normalized by its surface value is shown in Fig. 9 as a function of the normalized height z/H_{PBL} for the three regimes considered. As can be seen from the figure, the profiles are reasonably close to a straight line up to about 0.8 z/H_{PBL}. At about this height the normalized fluxes become negative, but their values still fall short of - 0.2, even though they are larger in absolute value than before since the shear helps to transport heat downwards at the top of the mixed layer.

(b) A real data example

The real data examples shown here were obtained using the Meso model with the step-mountain representation with coarse horizontal resolution of 80 km and 800 s time step. In the vertical, the model had 38 layers. The integration domain covered North America and adjacent waters. The only criterion for selecting the point and the time period for which to show the results was that a rather normal, preferably convectively driven PBL evolution not obscured by other weather phenomena be captured. This criterion was satisfied at Washington-Dulles airport during the first 12 hours of the forecast starting at 1200 UTC, June 14 1991. The change of the near surface temperature during the day was of the order of 15º C. From the point of view of weather phenomena that could interfere with the PBL evolution, the day was rather uneventful. It started with a small high over the area, and with the pressure gradually decreasing, the high disappeared by the afternoon.

The predicted temperature and the dew point temperature as functions of height are shown at two hour intervals in Fig. 10. The period covered by the vertical profiles is from 1200 to 2200 UTC. As can be seen from the rightmost panel, the wind changes the direction during the day, but remains weak throughout the lower troposphere. At the point considered, the height of the model topography is 182 m and there are 35 layers above the ground with the step-mountain representation. The interface between the lowest, and the second lowest model layer is at about 270 m, so that the middle of the lowest model layer, i.e., the lowest model level, is located about 225 m above mean sea level. The growth and warming of the neutral mixed layer with the capping inversion/increased stability layer on top is clearly visible in the figure.

The evolution of TKE over the first 12 hours of the forecast is shown in Fig. 11 for the ten lowest interfaces of the model layers. The lowest interface coincides with the ground surface, and at this interface the lower boundary condition is prescribed following MY82. The heights of the interfaces are indicated in the upper left corner of each diagram.

Generally, the large amplitude high frequency oscillations do not characterize the time evolution of TKE even with the time step as large as 800 s, although episodes of higher frequency oscillations can be seen particularly at higher levels. The wave with a four time step period seems to be dominant in the initial overshooting at interfaces 823 through 1219. Although this may be a coincidence, this period is comparable with the large eddy turn-over time. Another incidence of smaller amplitude, but higher frequency oscillation is visible in the later stages of the PBL development at the interfaces 1219 and 1447. Note that the oscillations at these two levels have opposite phases. Due to possible interference of other processes, however, it is hard to track the exact origin of this oscillation. Traces of the disturbances occurring at about the same time can be seen at all but the lowest level, suggesting that the actual cause may not be directly related to the turbulence scheme.

10. Conclusions

The implementation of the Mellor and Yamada Level 2.5 scheme in the NCEP Washington Meso model has been reconsidered in order to (i) identify the minimum conditions that enable satisfactory performance of the scheme for the full range of atmospheric forcing, and (ii) develop a robust, consistent, accurate and affordable computational procedure for application in synoptic

and subsynoptic scale models. What is meant here by the Level 2.5 scheme is the formulation discussed in MY82, and reproduced in Section 2 of this paper.

The aspects of the Level 2.5 scheme that were believed to be most relevant and/or most important, were carefully analyzed in order to achieve the first goal. The analysis revealed that it is sufficient to impose an appropriate upper limit on the master length scale, in addition to requiring that the turbulent kinetic energy (TKE) and the master length scale be positive. The upper limit proposed is proportional to the square root of twice the TKE and a function of large-scale buoyancy and shear parameters. In the unstable range this function is defined from the requirement that the TKE production be nonsingular in the case of growing turbulence, and in the stable range the function is derived from the requirement that the ratio of the vertical velocity deviation variance and TKE cannot be smaller than that corresponding to the regime of vanishing turbulence. In addition, a range of too strong stability and too weak shear has been identified where the TKE production is unable to balance the dissipation, so that the equilibrium solution for TKE becomes negative. This range is analogous to the range beyond the critical Richardson number in lower level models.

Accordingly, within the PBL the master length scale is estimated using the usual integral formula, and above the PBL it is computed as a fraction of the vertical grid size. The PBL height is defined as the height of the lowest model level at which the TKE production is unable to balance the dissipation, or alternatively, as the height of the lowest model level at which TKE approaches its prescribed lower bound. The values of the master length scale are then modified if necessary in order not to exceed the upper limit determined as explained.

Concerning the second goal, it is proposed that the TKE production/dissipation equation be solved iteratively over a time step, keeping the master length scale constant. In each iteration, the differential equation obtained by linearizing around the solution from the previous iteration is

solved. Two iterations appear to be sufficient for satisfactory accuracy, even with very long time steps and strong forcing. The computational cost of this procedure is minor. In the range where the TKE production is unable to balance the dissipation, the TKE and the master length scale are simply set to their lower bounds.

Finally, the empirical constants have been revised. The new set of constants is derived in the Appendix.

The modifications have been tested in off-line single column runs and in the Meso model. Choosing the examples illustrating the performance of the scheme, the emphasis was placed on convective boundary layers. It is sometimes argued that the Level 2.5 scheme has difficulties with the unstable stratification. Concerning the growth of the convective boundary layers, and the structures that developed, the results very much resemble the observations and textbook examples. No obvious major deficiencies of the scheme have been observed. The scheme has been implemented in the NCEP Meso model, and at other places where the model is used. The scheme is also available as one of the options in the MM5 model (communicated by Dudhia) and it has been used in general circulation studies (communicated by Bates).

APPENDIX

Determination of the constants in the Mellor-Yamada Level 2.5 model

Defining

$$F_B^2 = [u*^2 <\theta^2>/H^2], \tag{A1}$$

where $u*$ is the friction velocity, and H is the heat flux, MY82 Eq. (44f) may be rewritten as

$$B_2 = (B_1^{1/3}/Prt)\, F_B^2. \tag{A2}$$

An additional constraint relating the constants B_1 and B_2 referred to in MY82 is

$$R_B = B_1/B_2 = 3/2 \tag{A3}$$

which follows "from similarity considerations for decaying homogeneous temperature and velocity fields." Starting from the dynamical parameters, MY82 actually arrive at

$$R_B = B_1/B_2 = 16.6/10.1 = 1.64356443564, \tag{A4}$$

which agrees qualitatively with (A3). Note that the two constants, B_1 and B_2, could be obtained from (A2) and the prescription of the form (A3) or (A4). Then

$$B_1 = [(R_B\, F_B^2)/Prt]^{3/2}, \tag{A5}$$

and B_2 can be calculated either from (A2) or from (A3) or (A4) and the chosen value of R_B.

Strictly speaking, (A1) is not defined in the neutral limit. Moreover, as can be seen, e.g., from Zilitinkevitch (1970), Fig. 1.25, Yamada (1987), Fig. 4, different values for F_B are reached if the neutral stratification is approached from the stable and from the unstable side. The value proposed by MY82, and used here, is in between these two values. An alternative approach would be to choose different values of F_B for the stable and the unstable ranges, and thus define two different sets of constants for each of the two regimes. However, in order to avoid discontinuities, this would require an additional procedure for smooth matching of the two sets of constants at the neutral stratification. This may be a possible future extension of the model. In the meantime, however, a less ambitious attempt to specify an adequate set of constants is made.

Here, as in MY82,

$$\gamma_1 = 1/3\text{-}1/9 \tag{A6}$$

and

$$F_B = (3.167441983)^{1/2} \tag{A7}$$

are chosen. However, it is assumed that

$$Prt = 1. \tag{A8}$$

Using (A4),

$$R_B = B_1/B_2 = 16.6/10.1 = 1.64356443564,$$

from (A5)

$$B_1 = [(R_B F_B{}^2)/Prt]^{3/2} = 11.877992. \tag{A9}$$

From (A2)

$$B_2 = (B_1^{1/3}/Prt)\, F_B^2 = 7.226971, \tag{A10}$$

and from MY82 Eqs. (42a), (44d) and (44e), respectively,

$$A_1 = (B_1/2)(1/3 - \gamma_1) = 0.65988838, \tag{A11}$$

$$C_1 = \gamma_1 - 1/(3A_1)\, B_1^{-1/3} = 0.00083092297, \tag{A12}$$

$$A_2 = [A_1\, (\gamma_1 - C_1)]/(\gamma_1\, Prt) = 0.65742096. \tag{A13}$$

The turbulence model is not perfect, and not surprisingly, cannot fit all the observed data equally well. Thus, the velocity component variances obtained in the surface layer limit with the constants (A6)-(A13) do not compare with the measured values in the MY82 Table 1 as comfortably as the values obtained with the original MY82 constants. For example,

$$u/u* = 1.700636,$$

$$v/u* = w/u* = 1.075576,$$

$$q/u* = 2.2816429.$$

On the other hand, the modified set of constants result in other improvements that will be illustrated below.

The Mellor-Yamada Level 2 equivalent of the Monin-Obukhov function φ_M in the unstable range are shown in Fig. A1 for the original MY82 constants (empty squares) and the constants (A6)-(A13) (diamonds). As can be seen comparing Fig. 1 with MY82 Fig. 5a, a considerable improvement has been achieved with the new constants.

The Mellor-Yamada Level 2 equivalent of the Monin-Obukhov function φ_H in the unstable range are shown in Fig. A2 for the original MY82 constants (empty squares) and the constants (A6)-(A13) (diamonds). Careful examination of Fig. 2 and MY82 Fig. 5b again reveals an improvement with the new constants.

The Mellor-Yamada Level 2 equivalents of the Monin-Obukhov functions φ_M and φ_H in the stable range are shown in Figs. A3 and A4, respectively, for the original MY82 constants (empty squares) and the constants (A6)-(A13) (diamonds). As can be seen from the figures, and the MY82 Figs. 5a and 5b, this time the results are almost identical for φ_M, but considerable differences appear in the case of φ_H.

The ratio of the exchange coefficients for heat and momentum in the Mellor-Yamada Level 2 limit in the unstable range is shown in Fig. A5 as a function of the Richardson number Ri for the original MY82 constants (empty squares) and the constants (A6)-(A13) (diamonds). Note that there is a controversy about what this ratio should be in the unstable range. According to some Australian measurements (Zilitinkevitch 1970, Fig. 1.22; Garrat 1992) there is a strong dependence on stability, about twice stronger than that reached with the new set of constants. If these results are representative, as can be seen from Fig. A5, the constants (A6)-(A13) have still brought a considerable improvement. On the other hand, some Russian measurements indicate that the dependence on stability is weak, and that the ratio remains close to unity (Zilitinkevitch 1970, Fig. 1.22).

The ratio of the exchange coefficients for heat and momentum in the Mellor-Yamada Level 2 limit in the stable range is shown in Fig. A6 as a function of Richardson number *Ri* for the original MY82 constants (empty squares) and the constants (A6)-(A13) (diamonds). As can be verified by comparison with the data [e.g., Schumann (1991), Fig. 2; Zilitinkevitch (1970), Fig. 1.3], the results with the constants (A6)-(A13) agree well with the observations.

REFERENCES

Beljaars, A.C.M., 1994: The parameterization of surface fluxes in large-scale models under free convection. *Quart. J. Roy. Meteor. Soc.,* **121**, 255-270.

Canuto, V.M., F. Minotti, C. Ronchi, R.M. Ypma and O. Zeman, 1994: Second-order closure PBL model with new third-order moments: comparison with LES data. *J. Atmos. Sci.,* **51**, 1605-1618.

Chen, F., Z. Janjić and K. Mitchell, 1997: Impact of atmospheric surface-layer parameterization in the new land-surface scheme of the NCEP mesoscale Eta model. *Boundary-Layer Meteorology*, **48**, 391-421.

Deardorff, J.W., 1976: Clear and cloud-capped mixed layers - their numerical simulation, structure and growth and parameterization. *Seminars on the Treatment of the Boundary Layer in Numerical Weather Prediction,* ECMWF, Reading, U.K., 234-284. "Available from ECMWF, Shinfield Park, Reading, Berkshire RG2 9AX, U.K.'

Galperin, B., L.H. Kantha, S. Hassid and A. Rosati, 1988: A quasi-equilibrium turbulent energy model for geophysical flows. *J. Atmos. Sci.,* **45**, 55-62.

Garrat, J.R., 1992: The Atmospheric Boundary Layer. *Cambridge University Press,* 316 pp.

Gerrity, J.P. Jr., T.L. Black and R.E. Treadon, 1994: The numerical solution of the Mellor-Yamada level 2.5 turbulent kinetic energy equation in the Eta model. *Mon. Wea Rev.,* **122**, 1640-1646

Helfand, H.M., and J.C. Labraga, 1988: Design of a nonsingular level 2.5 second-order closure model for the prediction of atmospheric turbulence. *J. Atmos. Sci.,* 45, 113-132.

Holtslag, A.A. and Chin-Hoh Moeng, 1991: Eddy diffusivity and countergradient transport in the convective atmospheric boundary layer. *J. Atmos. Sci.,* **48**, 1690-1698.

Janjić, Z.I., 1979: Forward-backward scheme modified to prevent two-grid-interval noise and its application in sigma coordinate models. *Contrib. Atmos. Phys.,* **52**, 69-84.

Janjić, Z.I., 1984: Non-linear advection schemes and energy cascade on semi-staggered grids. *Mon. Wea. Rev.,* **112**, 1234-1245.

Janjić, Z.I., 1990: The step-mountain coordinate: physical package. *Mon. Wea. Rev.*, **118**, 1429-1443.

Janjić, Z.I., 1994: The step-mountain eta coordinate model: further developments of the convection, viscous sublayer and turbulence closure schemes. *Mon. Wea. Rev*., **122**, 927-945.

Janjić, Z.I., 1996: The surface layer in the NCEP Eta Model. Eleventh Conference on Numerical Weather Prediction, Norfolk, VA, 19-23 August 1996; Amer. Meteor. Soc., Boston, MA, 354-355.

Lobocki, L., 1993: A procedure for the derivation of surface-layer bulk relationships from simplified second order closure models. *J. Appl.Meteor.,* **32**, 126-138.

Mellor, G.L. and T. Yamada, 1982: Development of a turbulence closure model for geophysical fluid problems. *Rev. Geophys. Space Phys.,* **20**, 851-875.

Mason, P.J., 1989: Large-eddy simulation of the convective boundary layer. *J. Atmos. Sci*, **46**, 1492-1516.

Mesinger, F., Z.I. Janjić, S. Ničković, D. Gavrilov and D.G. Deaven, 1988: The step-mountain coordinate: model description and performance for cases of Alpine lee cyclogenesis and for a case of Appalachian redevelopment. *Mon. Wea. Rev.,* **116**, 1493-1518.

Monin, A.S. and A.M. Obukhov, 1954: Basic laws of turbulent mixing in the surface layer of the atmosphere. *Contrib. Geophys. Inst. Acad. Sci. USSR,* (151), 163-187 (in Russian).

Paulson, C.A., 1970: The mathematical representation of wind speed and temperature profiles in the unstable atmospheric surface layer. *J. Appl. Meteor.,* **9**, 857-861.

Schumann, U., 1991: Subgrid length-scales for large-eddy simulation of stratified turbulence. *Theoret. Comput. Fluid Dynamics,* **2**, 279-290.

Yamada, N., 1986: Examination of Schumann's method of judging the realizability of turbulence closure models. *Bound.-Layer Meteor.,* **37**, 415-419.

Yamada, N., 1987: A trial prediction of the values of some surface-layer turbulence constants using Schumann's method for promoting realizability. *Bound.-Layer Meteor.*, **38**, 1-15.

Zhao, Q. and F.H. Carr, 1997: A prognostic cloud scheme for operational NWP models. *Mon. Wea. Rev.,* **125**, 1931-1953.

Zilitinkevitch, S.S., 1970: Dynamics of the Planetary Boundary Layer. Gidromet. Izdat., Leningrad, 292 pp. (in Russian)

Zilitinkevich, S.S., 1995: Non-local turbulent transport: pollution dispersion aspects of coherent structure of convective flows. In: Air Pollution III - Volume I. *Air Pollution Theory and Simulation* (Eds. H. Power, N. Moussiopoulos and C.A. Brebbia). Computational Mechanics Publications, Southampton Boston, 53-60.

FIGURE CAPTIONS

Fig. 1. Solutions of the non-singularity condition equation (4.8) p_1 (upper panel) and p_2 (lower panel) for a very wide range of g_H and g_M [$\pm 1^o$ K m^{-1} and (2 m s^{-1} m^{-1})^2].

Fig. 2. Solutions of the equilibrium equation (4.9) s_1 (upper panel) and s_2 (lower panel) for a very wide range of g_H and g_M [$\pm 1^o$ K m^{-1} and (2 m s^{-1} m^{-1})^2].

Fig. 3. Values of the upper bound $1/p_1$ for $p_1 \geq 0$. The values for a very wide range of g_H and g_M are shown [$\pm 1^o$ K m^{-1} and (2 m $^{-1}$ m^{-1})^2].

Fig. 4 Solutions of (5.6) t_1 (left panel) and t_2 (right panel) for $R_{SL}=(1+10^{-12})R_S$, and a wide range in the stable part of the g_H x g_M plane [1^o K m^{-1} and (2 m s^{-1} m^{-1})^2].

Fig. 5. Free convection: averaged vertical distribution of the turbulent exchange coefficient for heat K_H normalized by the product of $w*$ and H_{PBL} as a function of the normalized height z/H_{PBL} for BL height and surface buoyancy flux exceeding 500 m, and 100 W m^{-2}.

Fig. 6. Free convection: average profiles of K_H normalized by the product of $w*$ and H_{PBL} for PBL height and surface buoyancy flux exceeding 1000 m and 100 W m^{-2} (squares), maximum height of PBL and surface buoyancy flux greater than 100 W m^{-2} (triangles) and the profile of Fig. 5 (circles).

Fig. 7. Free convection: average profiles of the buoyancy flux normalized by the surface buoyancy flux for PBL height and surface buoyancy flux exceeding 500 m and 100 W m^{-2} (circles), PBL height and surface buoyancy flux exceeding 1000 m and 100 W m^{-2} (squares), maximum height of PBL and surface buoyancy flux greater than 100 W m^{-2} (triangles).

Fig. 8. Convective PBL with shear: average profiles of K_H normalized by the product of $w*$ and H_{PBL} for PBL height and surface buoyancy flux exceeding 500 m and 100 W m^{-2} (circles), PBL height and surface buoyancy flux exceeding 1000 m and 100 W m^{-2} (squares), and PBL height greater than or equal to 1965 m and surface buoyancy flux exceeding 100 W m^{-2} (triangles).

Fig. 9. Convective PBL with shear: average profiles of the buoyancy flux normalized by the surface buoyancy flux for the PBL height and surface buoyancy flux exceeding 500 m and 100 W m^{-2} (circles), the PBL height and surface buoyancy flux exceeding 1000 m and 100 W m^{-2} (squares), and the PBL height greater than or equal to 1965 m and the surface buoyancy flux exceeding 100 W m^{-2} (triangles).

Fig. 10. The forecast temperature and the dew point profiles at the Washington-Dulles airport at two hour intervals from 1200 to 2200 UTC, June 14 1991. The wind is shown in the rightmost panel.

Fig. 11. Evolution of TKE over 12 hours at ten lowest interfaces of the model layers. The heights of the interfaces are indicated in the upper left corner of each time series.

Fig. A1. The Mellor-Yamada Level 2 equivalent of the Monin-Obukhov function φ_M in the unstable range for the original MY82 constants (empty squares) and the constants (A6)-(A13) (diamonds).

Fig. A2. The Mellor-Yamada Level 2 equivalent of the Monin-Obukhov function φ_H in the unstable range for the original MY82 constants (empty squares) and the constants (A6)-(A13) (diamonds).

Fig. A3. The Mellor-Yamada Level 2 equivalents of the Monin-Obukhov functions φ_M in the stable range for the original MY82 constants (empty squares) and the constants (A6)-(A13) (diamonds).

Fig. A4. The Mellor-Yamada Level 2 equivalents of the Monin-Obukhov functions φ_H in the stable range for the original MY82 constants (empty squares) and the constants (A6)-(A13) (diamonds).

Fig. A5. The ratio of the exchange coefficients for heat and momentum in the Mellor-Yamada Level 2 limit in the unstable range as a function of Richardson number *Ri* for the original MY82 constants (empty squares) and the constants (A6)-(A13) (diamonds).

Fig. A6. The ratio of the exchange coefficients for heat and momentum in the Mellor-Yamada Level 2 limit in the stable range as a function of Richardson number *Ri* for the original MY82 constants (empty squares) and the constants (A6)-(A13) (diamonds).

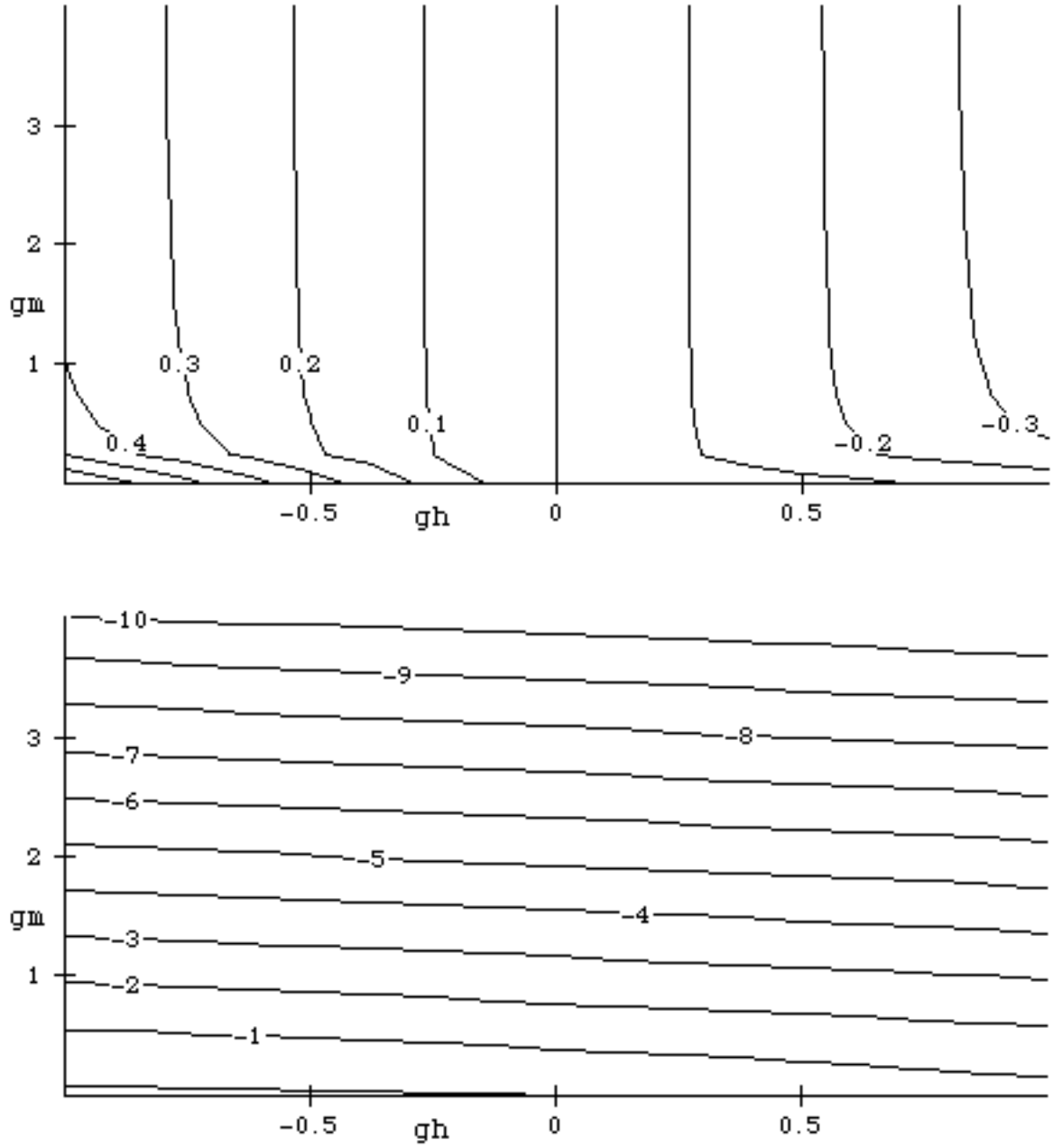

Fig. 1. Solutions of the non-singularity condition equation (4.8) p_1 (upper panel) and p_2 (lower panel) for a very wide range of g_H and g_M [$\pm 1^o$ K m^{-1} and (2 m s^{-1} m^{-1})^2].

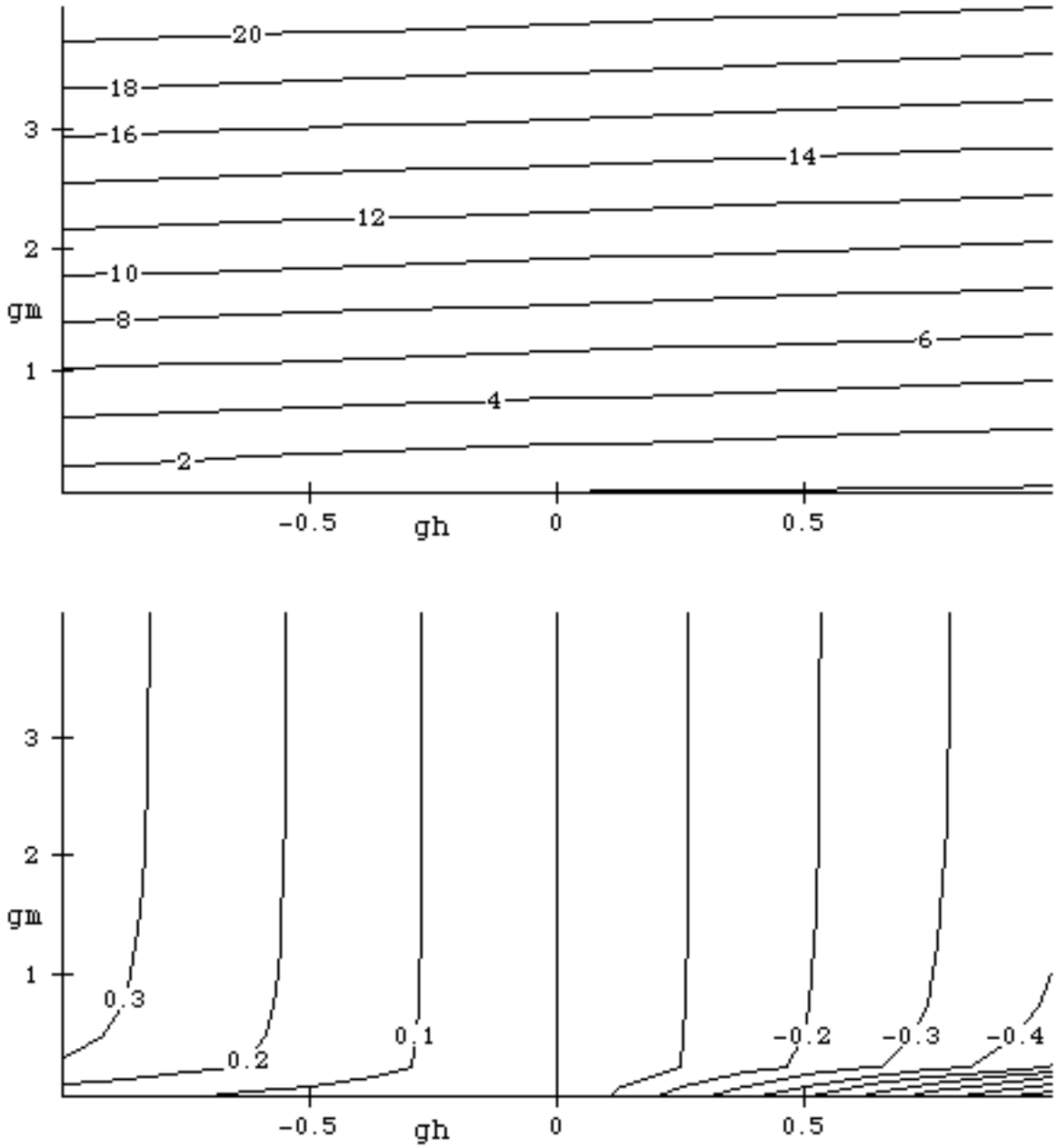

Fig. 2. Solutions of the equilibrium equation (4.9) s_1 (upper panel) and s_2 (lower panel) for a very wide range of g_H and g_M [$\pm 1^o$ K m^{-1} and (2 m s^{-1} m^{-1})^2].

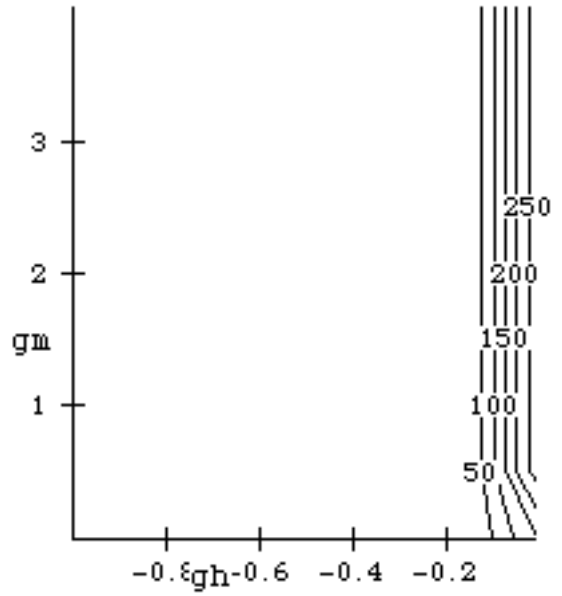

Fig. 3. Values of the upper bound $1/p_1$ for $p_1 \geq 0$. The values for a very wide range of g_H and g_M are shown [$\pm 1^\circ$ K m^{-1} and $(2\ m^{-1}\ m^{-1})^2$].

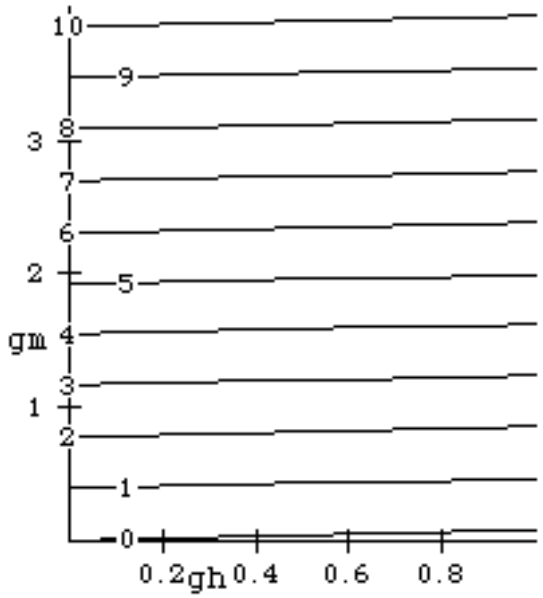
10
9
3
8
7
6
2
5
gm
4
3
1
2
1
0
0.2gh
0.4
0.6
0.8

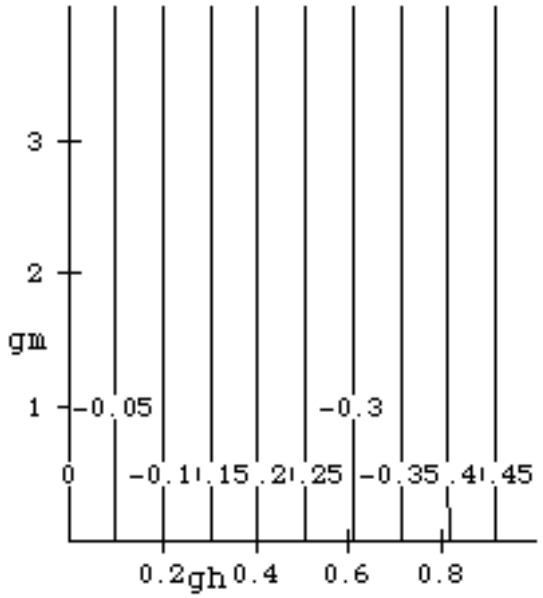
3
2
gm
1
-0.05
-0.3
0
-0.1
.15
.2
.25
-0.35
.4
.45
0.2gh
0.4
0.6
0.8

Fig. 4 Solutions of (5.6) t_1 (left panel) and t_2 (right panel) for $R_{sL}=(1+10^{-12})R_s$, and a wide range in the stable part of the g_H x g_M plane [1° K m^{-1} and (2 m s^{-1} m^{-1})^2].

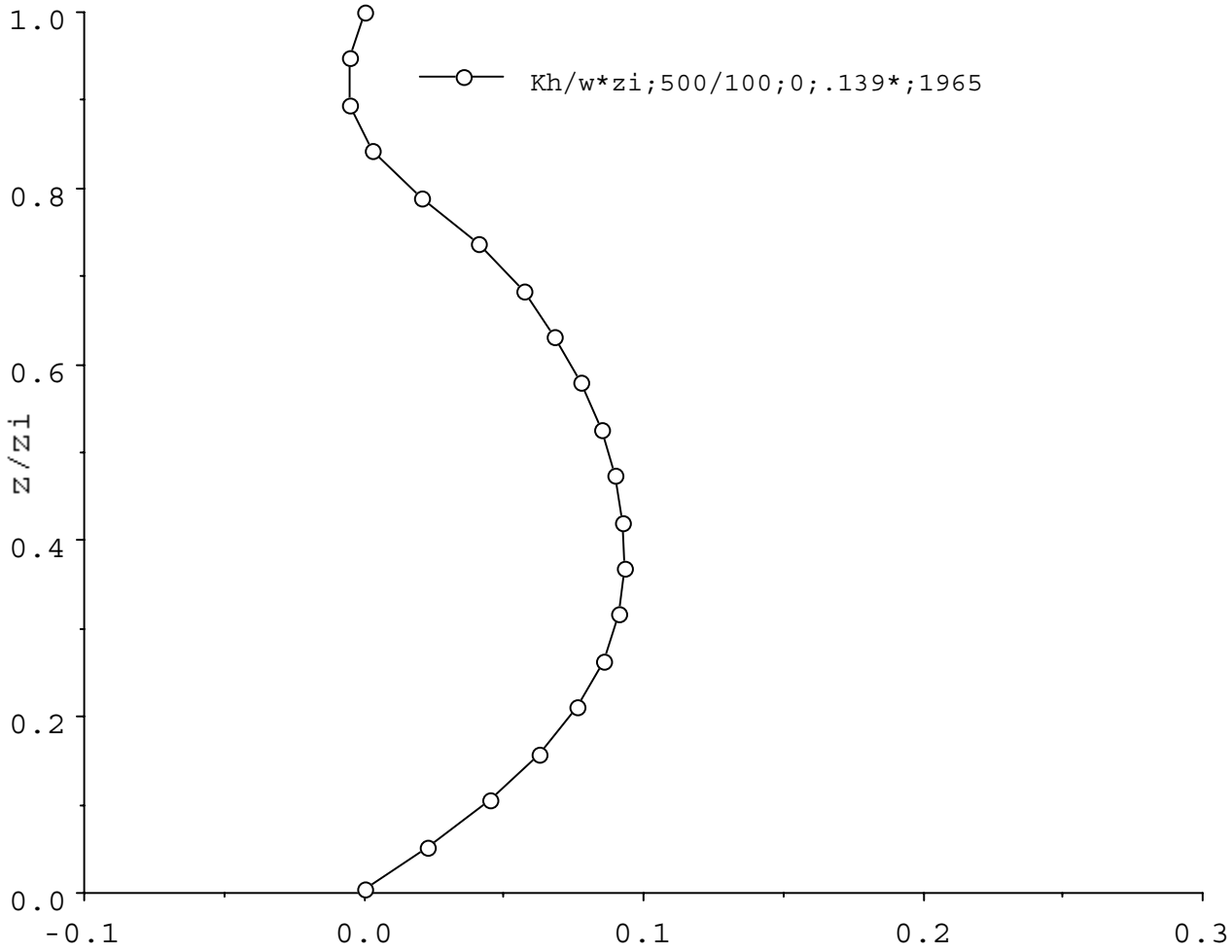

Fig. 5. Free convection: averaged vertical distribution of the turbulent exchange coefficient for heat K_H normalized by the product of w∗ and H_{PBL} as a function of the normalized height z/H_{PBL} for BL height and surface buoyancy flux exceeding 500 m, and 100 W m^{-2}.

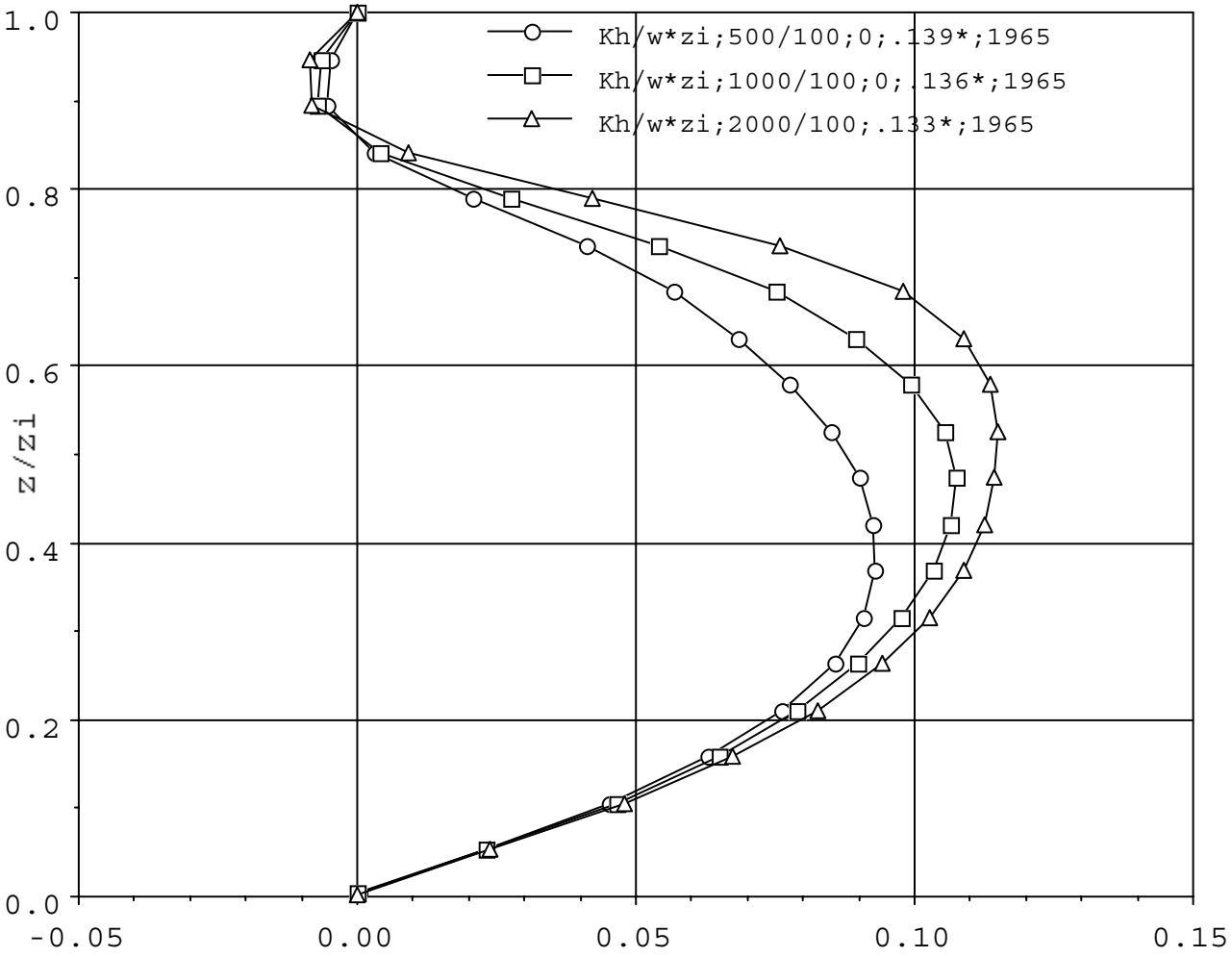

Fig. 6. Free convection: average profiles of K_H normalized by the product of $w*$ and H_{PBL} for PBL height and surface buoyancy flux exceeding 1000 m and 100 W m^{-2} (squares), maximum height of PBL and surface buoyancy flux greater than 100 W m^{-2} (triangles) and the profile of Fig. 5 (circles).

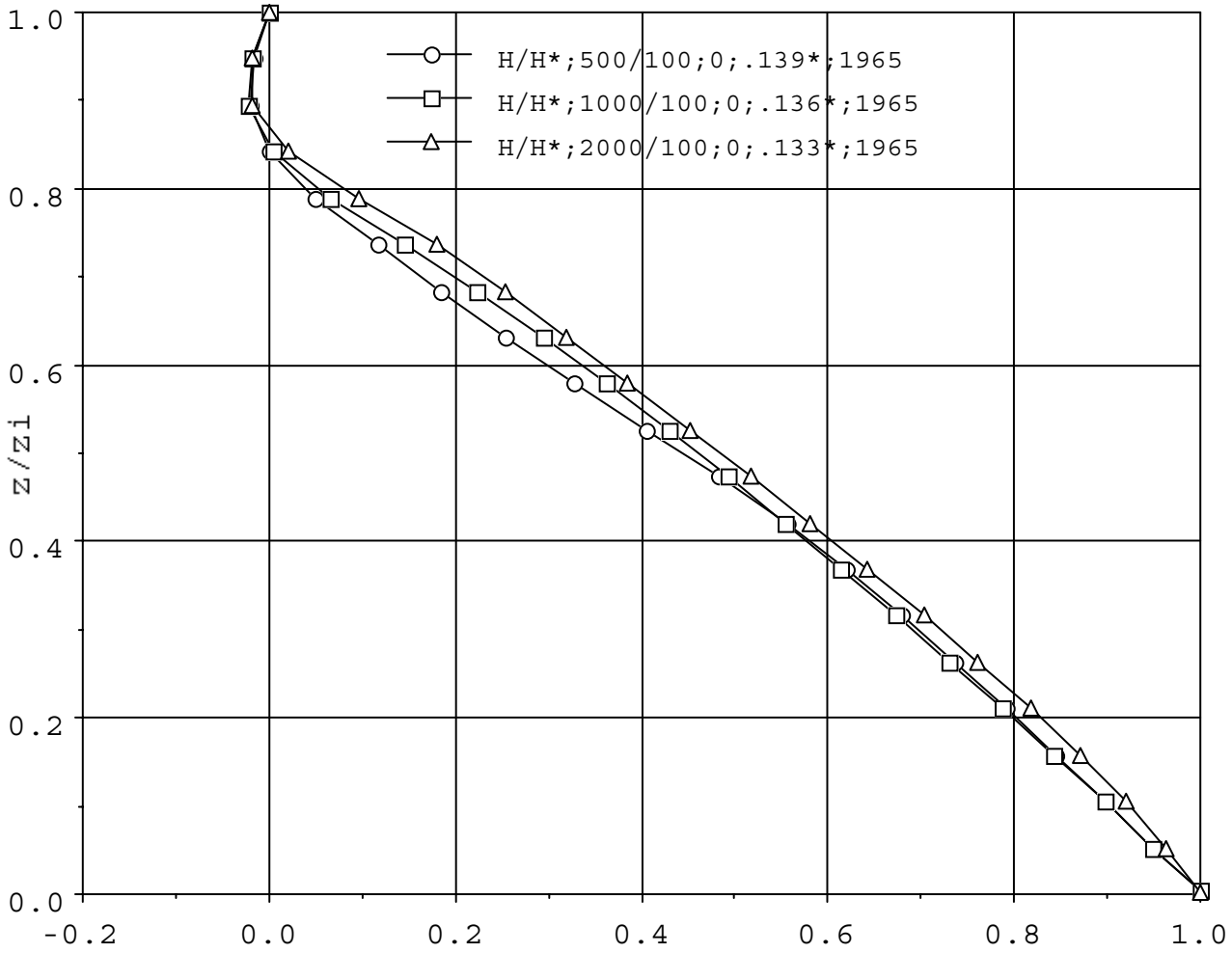

Fig. 7. Free convection: average profiles of the buoyancy flux normalized by the surface buoyancy flux for PBL height and surface buoyancy flux exceeding 500 m and 100 W m^{-2} (circles), PBL height and surface buoyancy flux exceeding 1000 m and 100 W m^{-2} (squares), maximum height of PBL and surface buoyancy flux greater than 100 W m^{-2} (triangles).

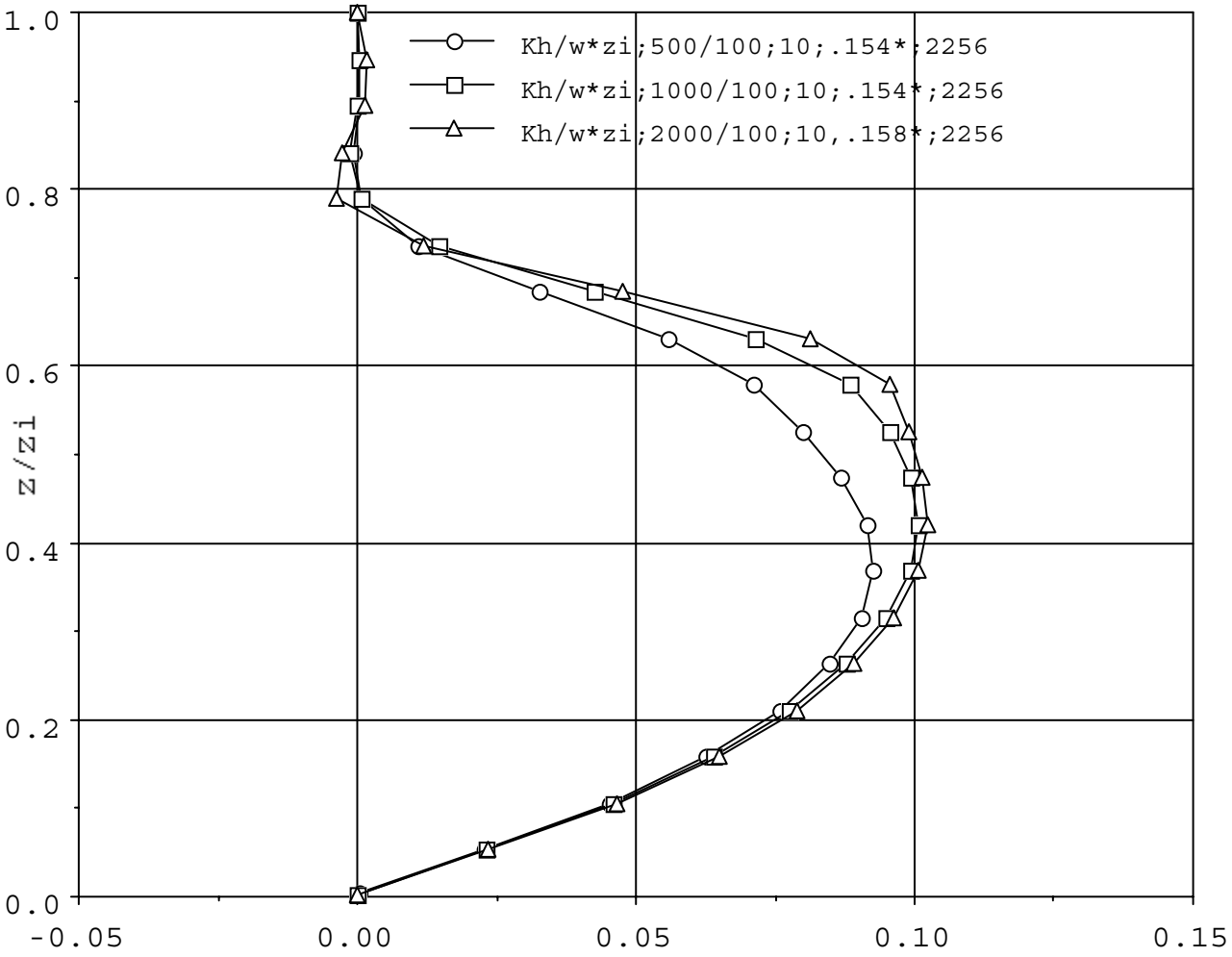

Fig. 8. Convective PBL with shear: average profiles of K_H normalized by the product of $w*$ and H_{PBL} for PBL height and surface buoyancy flux exceeding 500 m and 100 W m^{-2} (circles), PBL height and surface buoyancy flux exceeding 1000 m and 100 W m^{-2} (squares), and PBL height greater than or equal to 1965 m and surface buoyancy flux exceeding 100 W m^{-2} (triangles).

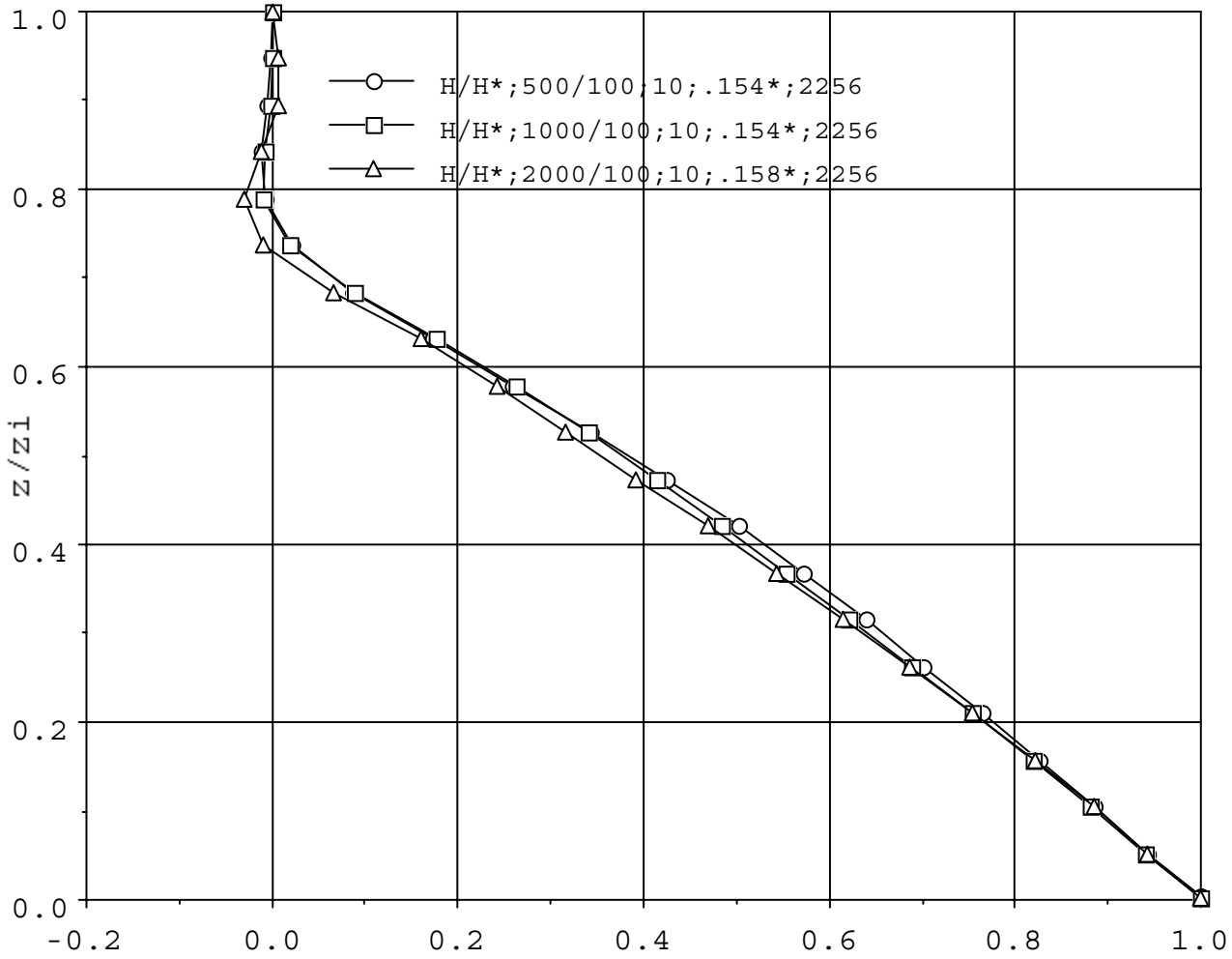

Fig. 9. Convective PBL with shear: average profiles of the buoyancy flux normalized by the surface buoyancy flux for the PBL height and surface buoyancy flux exceeding 500 m and 100 W m^{-2} (circles), the PBL height and surface buoyancy flux exceeding 1000 m and 100 W m^{-2} (squares), and the PBL height greater than or equal to 1965 m and the surface buoyancy flux exceeding 100 W m^{-2} (triangles)..

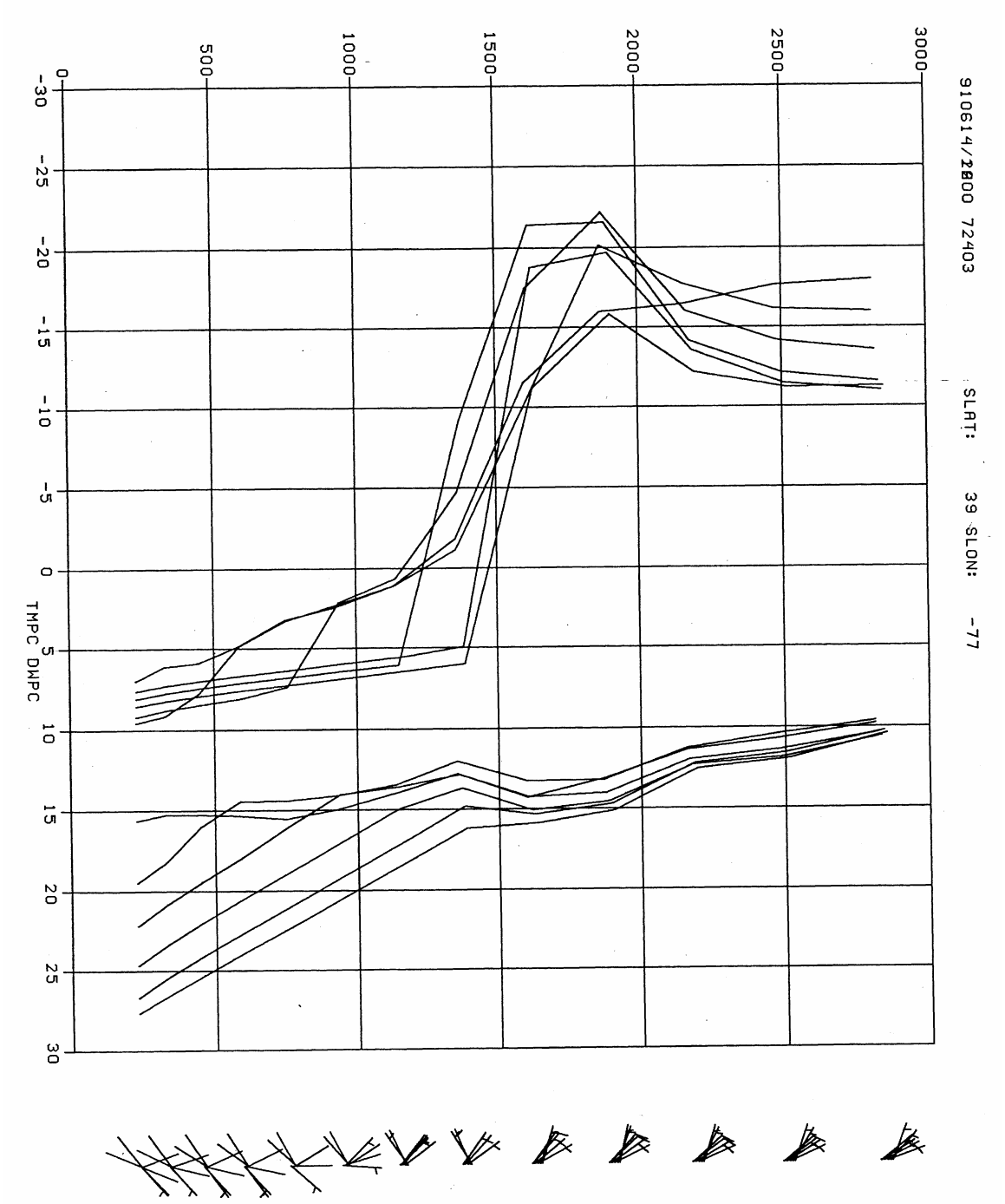

Fig. 10. The forecast temperature and the dew point profiles at the Washington-Dulles airport at two hour intervals from 1200 to 2200 UTC, June 14 1991. The wind is shown in the rightmost panel.

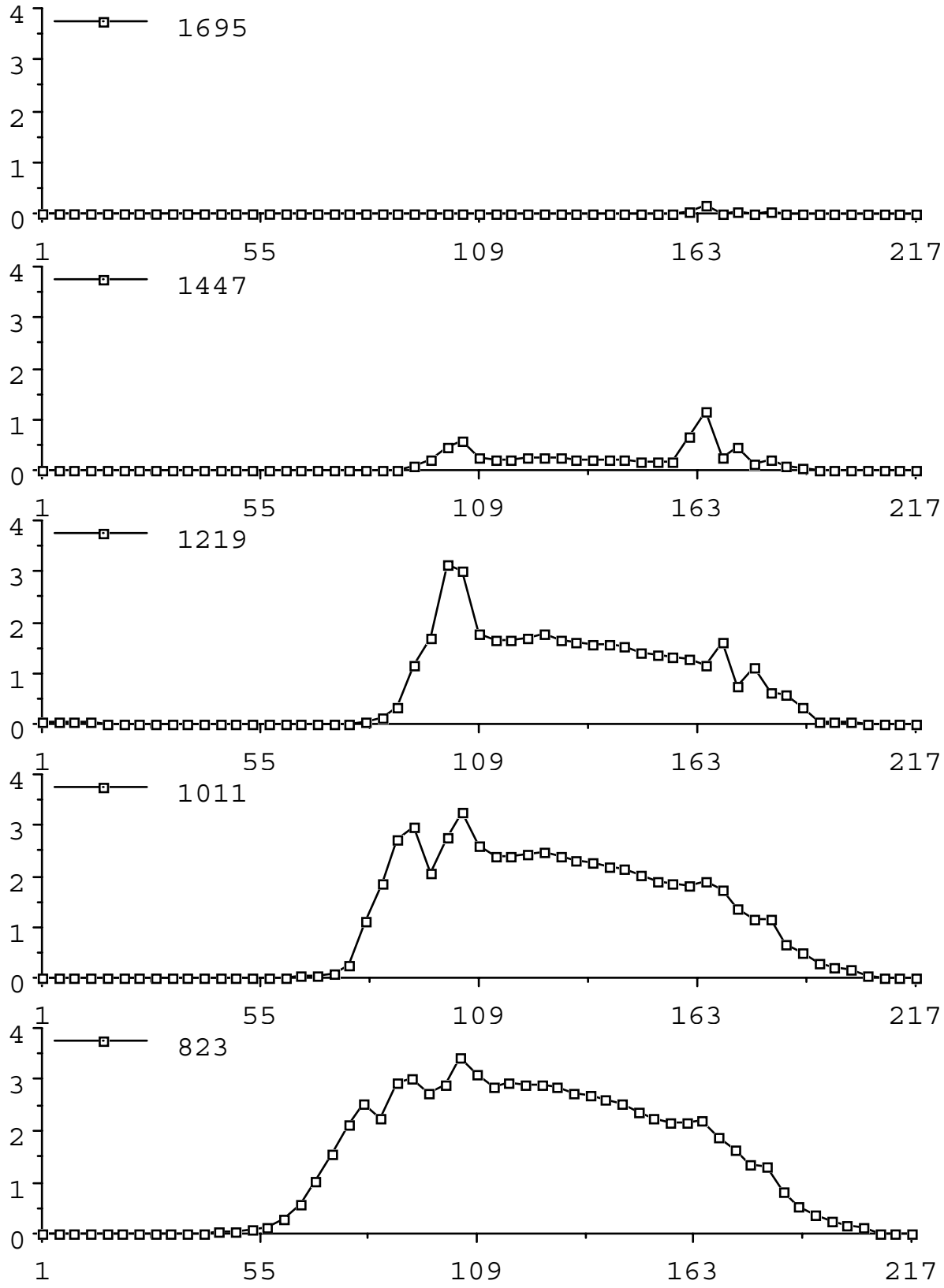

- Continued on next page -

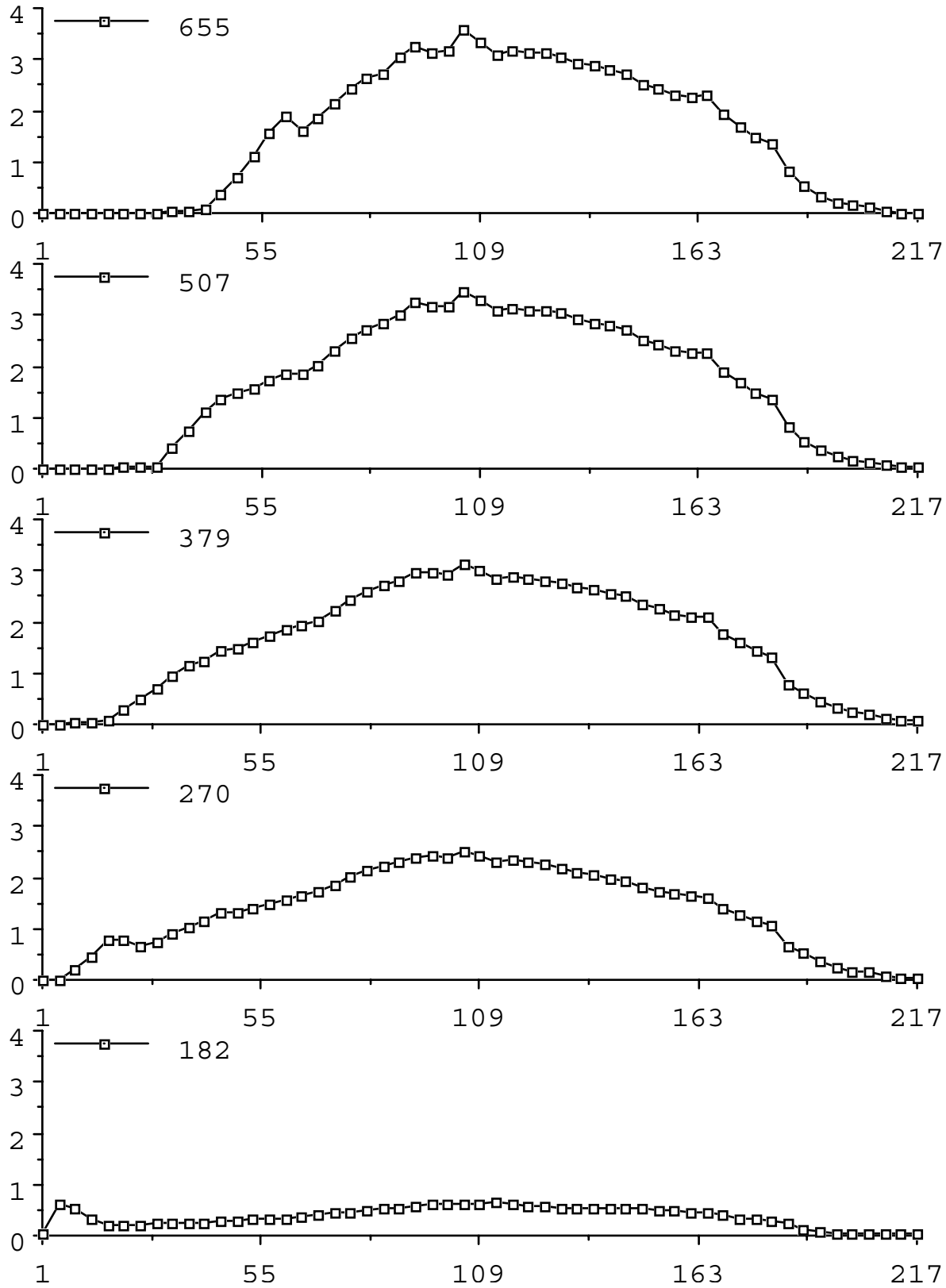

Fig. 11. Evolution of TKE over 12 hours at ten lowest interfaces of the model layers. The heights of the interfaces are indicated in the upper left corner of each time series.

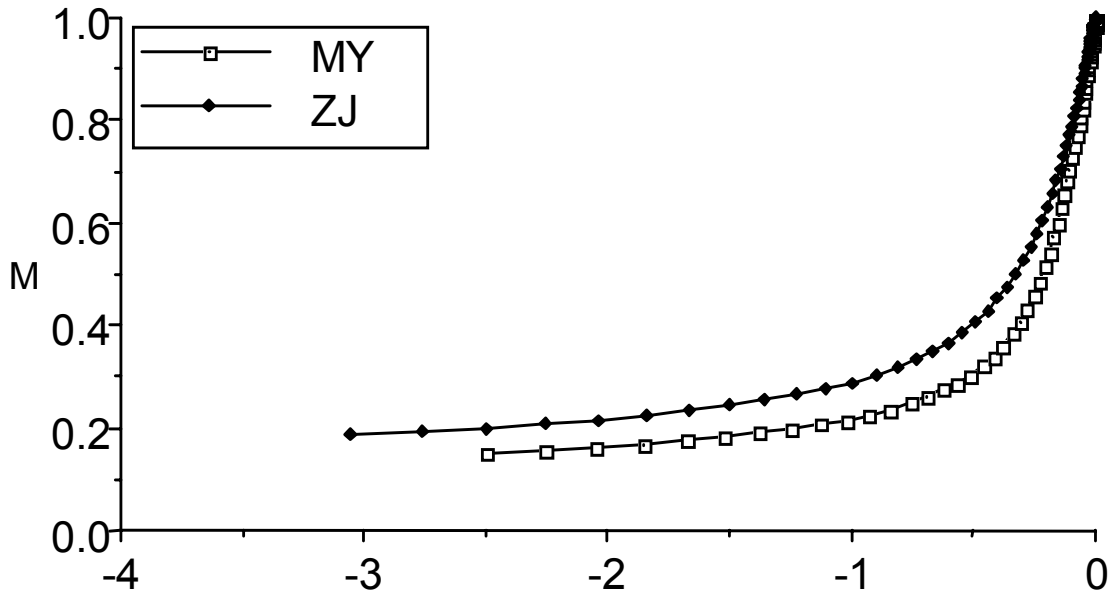

Fig. A1. The Mellor-Yamada Level 2 equivalent of the Monin-Obukhov function φ_M in the unstable range for the original MY82 constants (empty squares) and the constants (A6)-(A13) (diamonds).

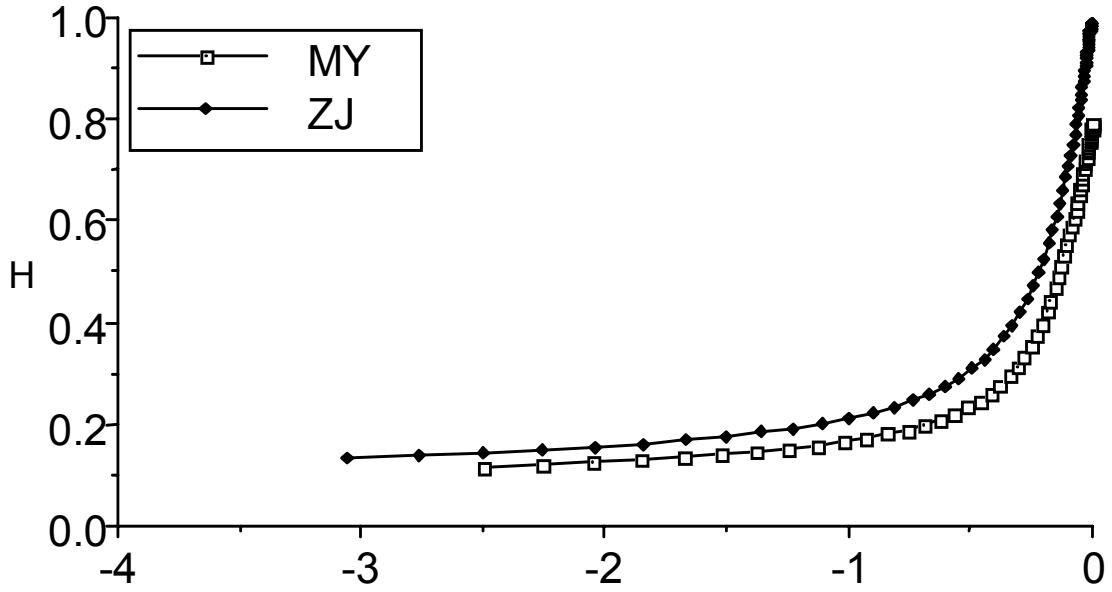

Fig. A2. The Mellor-Yamada Level 2 equivalent of the Monin-Obukhov function φ_H in the unstable range for the original MY82 constants (empty squares) and the constants (A6)-(A13) (diamonds).

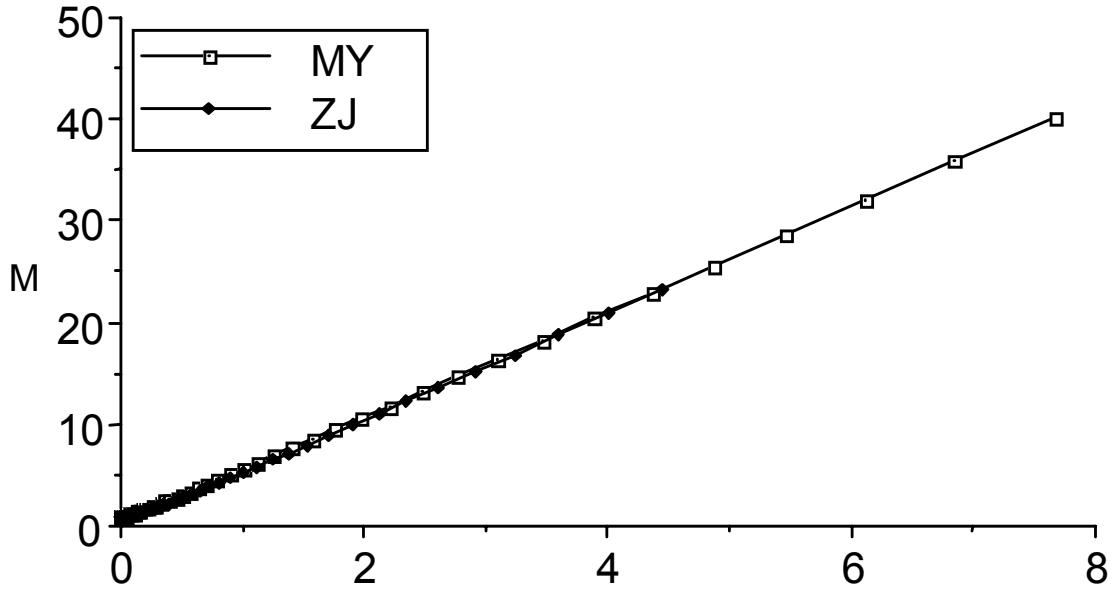

Fig. A3. The Mellor-Yamada Level 2 equivalents of the Monin-Obukhov functions φ_M in the stable range for the original MY82 constants (empty squares) and the constants (A6)-(A13) (diamonds).

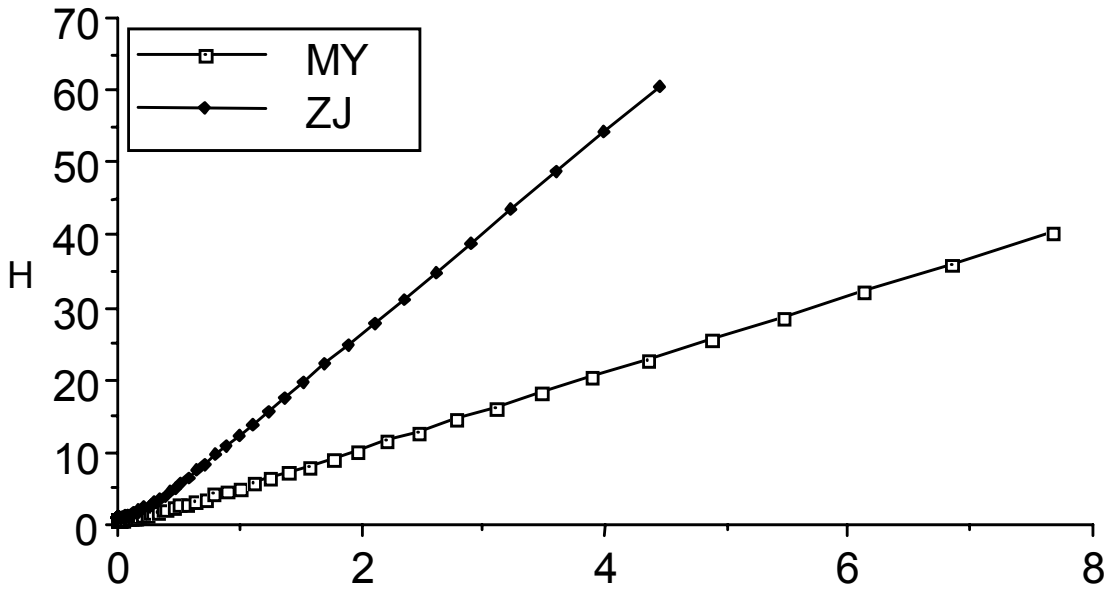

Fig. A4. The Mellor-Yamada Level 2 equivalents of the Monin-Obukhov functions φ_H in the stable range for the original MY82 constants (empty squares) and the constants (A6)-(A13) (diamonds).

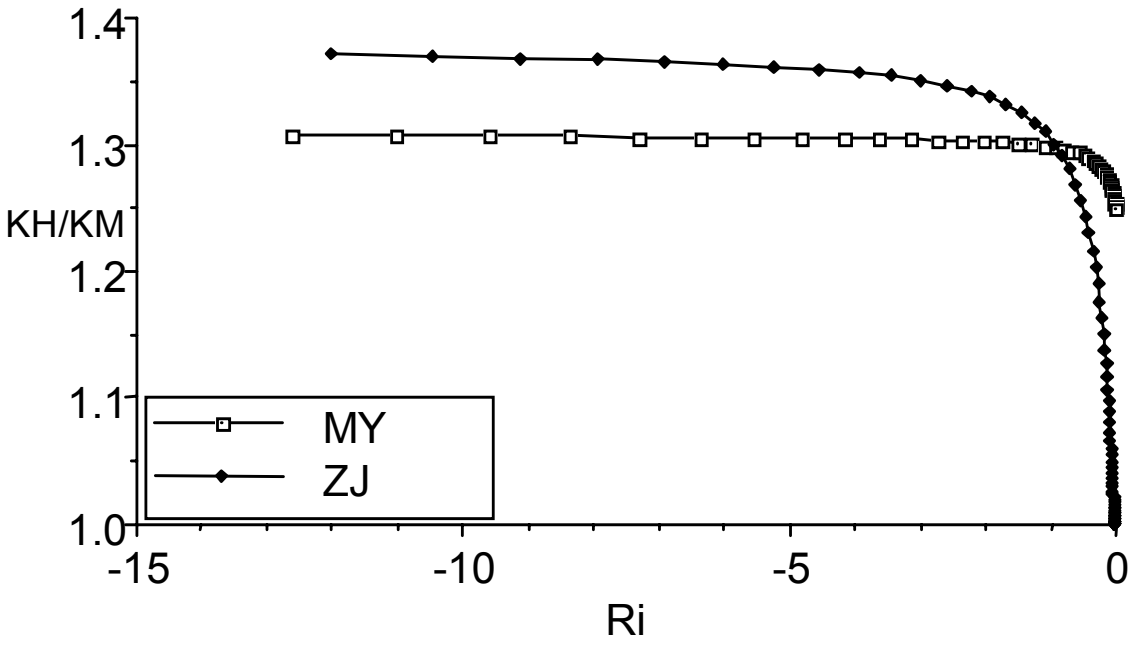

Fig. A5. The ratio of the exchange coefficients for heat and momentum in the Mellor-Yamada Level 2 limit in the unstable range as a function of Richardson number Ri for the original MY82 constants (empty squares) and the constants (A6)-(A13) (diamonds).

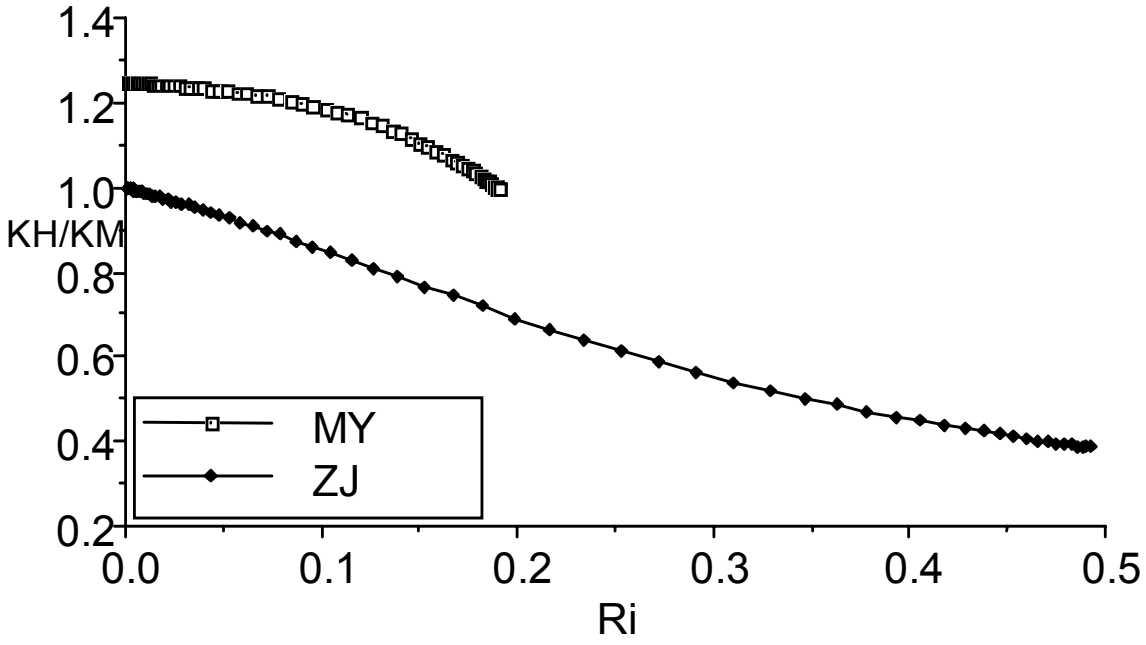

Fig. A6. The ratio of the exchange coefficients for heat and momentum in the Mellor-Yamada Level 2 limit in the stable range as a function of Richardson number *Ri* for the original MY82 constants (empty squares) and the constants (A6)-(A13) (diamonds).